Doctoral Dissertation
博士学位論文

Theoretical Study of Astatine-Gold Surface Interaction for Radiotherapy Applications
(核医学治療薬開発のためのアスタチン―金表面相互作用に関する理論的研究)

TANUDJI JEFFREY
タヌジー ジェフリー

July 2024

Division of Precision Engineering and Applied Physics
Graduate School of Engineering
Osaka University

大阪大学大学院工学研究科
精密・応用物理学専攻

Abstract

Cancer begins as an aberration of the DNA that fails to undergo cell death. As it grows, the abnormal cells take in energies meant for healthy cells and this causes stress on the body of the patient. Recent developments look at a generalized treatment involving heavier radionuclides to target cancer masses. This type of treatment is called the targeted alpha therapy or TAT and uses the alpha decay of heavier radioisotopes in order to disrupt the growth of cells. The alpha particle, being heavier than electrons and having a larger energy, can cut DNAs more effectively and cause the cell to die.

The use of astatine as radionuclide stems from the certainty of it releasing an alpha particle during its decay and its relatively short half-life. However, randomly releasing astatine into a patient's body may cause more harm than benefit as it can target healthy organs. It therefore must be carried by some material that can hold the astatine until they reach the targeted areas and be biocompatible. Gold, in the form of gold nanoparticles, is chosen for this purpose for its known biocompatibility as well as other advantageous properties that could be used against cancer.

Information obtained from experiments show that astatine can indeed be adsorbed by gold, but these experiments are geared towards the medical field, which is interested in the efficacy of the treatment. This study is conducted in order to support the initiative by theoretically simulating the carrier system to look at the fundamental science behind this adsorption phenomenon. By doing this, the hope is to be able to recommend to experimentalists and the medical community on the optimum shape and size the carrier particles should be for further investigation.

The first part of this work looks at the physical mechanism for astatine adsorption on gold. The Au(111) is chosen as the test slab since the surface is well known for being the most stable among the other surface facets. Astatine is found to adsorb on the fcc-hollow site and that the adsorption process is based on covalent bonding. Evidence for hybridization of the 6p orbital of astatine with the 5d and 6s orbitals of gold also support this finding, as well as the lack of any charge transfers between astatine and gold. The addition of van der Waals (vdW) and spin orbit coupling (SOC) corrections provide more accurate information.

The second part of this work deals with the comparison between astatine and iodine when adsorbed on Au(111). Since astatine is a halogen, the comparison between another halogen element that has been in use for longer can provide us with insights as to the peculiarities of astatine. The first anomaly is that astatine adsorbs stronger on gold than iodine. This is normally not the case since adsorption energies tend to decrease the lower the element is in the periodic table. However, the presence of a fully occupied 4f orbital means that a phenomenon known as lanthanide contraction is affecting the physics of astatine. Due to astatine being lower in the periodic table than iodine, electrons have to occupy the 4f orbitals before filling the valence orbitals. The 4f orbital is known for its less effective screening of core charges, making the valence electrons more susceptible to the attraction from the nucleus.

The final part of this work concerns the design of surfaces. Actual surfaces are not pristine and therefore may be subject to a number of defects. Furthermore, the three-dimensional nature of gold nanoparticles means there would be different surface facets, including stepped surfaces. An extension to the Au(111), the Au(211) introduces a step into the flat surface, making the facet more

representative of a three-dimensional shape. Both astatine and iodine adsorb on the edge-bridge site on Au(211), with stronger adsorption energies than on Au(111). This is due to the work function of Au(211) being smaller than Au(111), meaning Au(211) is more active. Au(211) also provides a more stable adsorption for the adsorbates, since the energy required to dislodge the adsorbate from the edge-bridge site is higher than the energy required for Au(111). The charge movements and densities of states were looked at and they showed few differences between the Au(111) and the Au(211). This confirms the stronger adsorption is caused by the surface facet.

The future developments in this field can benefit greatly from the addition of theoretical calculation methods. Various designs can first be evaluated theoretically before going through experimental verification. Considering the current state of availability, theoretical methods can be employed to find the most promising samples which warrant further testing. Finally, different materials and radionuclides can be studied, depending on the conditions that may be desired by the medical community. These are just several future ideas that can be realized with theoretical methods. As more researchers employ these techniques, important discoveries can be made which can support the medical community.

Table of contents

Chapter 1

Introduction

1.1 Background

Cancer is a leading cause of death; in 2022, it was projected that almost 10 million people died due to cancer [1]. The main cause of cancer is a genetic aberration that affects the way our cells regenerate [2]. Currently, there are several types of treatments that can be done on the patient: these are surgery, chemical treatment (chemotherapy), and radiation treatment [3]. Each case will have its own advantages and disadvantages, and in the end it falls to the patient to decide which one he/she will choose.

1.1.1 Radiotherapy

Radioactivity was discovered in the late 19th century by Henri Becquerel when he was doing research on phosphorescent materials [4]. During this time, several pioneers on the subject emerged, such as Wilhelm Röntgen, Marie and Pierre Curie, and Ernst Rutherford, who performed experiments on the nature and applications of radioactivity. Of interest is one of the natures of such phenomenon, which is the emission of "energetic particles" [5]. Some of these particles were discovered by Rutherford and named α-particles and β-particles (helium ions and electrons respectively) and would play a part in the development of nuclear medicine.

There are two types of radiotherapy, external and internal. External treatments employ radiation from outside sources (normally X-rays or gamma-rays) to target affected areas [6]. Its nature allows treatment in areas that are difficult to reach or areas where surgery would be risky, such as the brain and spine [7]. These methods require the patients to be in the medical facility for each treatment since the equipment cannot be moved around. On the other hand, internal treatments do not require continuous presence in medical facilities. The treatments are placed in the patients' bodies and continue to work until some determined time.

The feasibility of internal nuclear medicine was shown in 1946 when Drs. Saul Hertz and Arthur Roberts reported radioactive iodine, a β emitter, as an effective cure for thyroid cancer [8]. Aside from directly treating the cancerous cells, some radioactive iodines can be used as tracers, allowing for the tracking of anything that the radionuclide is attached to inside the patient [9]. Several studies have confirmed the efficacy of radioactive iodine such as iodine-123 and iodine-125 in acting as tracers and medicine in treating cancers [9-11].

1.1.2. Astatine for radiotherapy

There are several issues that can occur using these β emitters. For one, the β emitters are not always reliable. These radionuclides do not always emit β-particles; sometimes γ-particles are emitted and this may pose unintended radiation to healthy cells. The other is the possibility of β radiation resistance, in which the newly formed cancer cells are more resistant to the β radiation treatment [12].

Recently, heavier radioactive elements are being used in place of iodine as radioactive source. These elements release α-particles (He^{2+} ions), which are becoming more attractive, since the α-particles' high Linear Energy Transfer value compared to β-particles allow for a more effective treatment [12-14]. Currently, astatine-211 (^{211}At) is being studied in the hopes of adding another arsenal in the fight against cancer.

There are several reason why ^{211}At is chosen for this treatment. For one, it has a short half-life of 7.2 hours, meaning the treatment does not stay in the body for very long [14,15]. Additionally, the decay of astatine always provides one α-particle. These characteristics make it unique among the other astatine isotopes, which may not produce α-particles or decays too quickly to be of any use [16].

Unfortunately, employing ^{211}At directly to treat cancer masses does not ensure the radionuclides can reach the target area. It must be attached to some kind of carrier, which can also be appended with some targeting compound, to deliver it to the intended location and prevent it from being absorbed by healthy organs.

1.1.3 Gold as material for carrier

As a substance, gold is inert, which makes it less likely to react with other biological compounds [17]. This has been shown in biological experiments in which gold, in the form of gold nanoparticles (AuNPs), is employed due to its biocompatibility [19-22]. Additionally, the use of gold has several properties that are beneficial, such as surface plasmon resonance, causing biological radiosensitization to targeted cells, catalyzing the production of reactive oxygen species [19, 22-24]. These additional capabilities allow gold to be useful in cancer treatments.

Another reason to employ gold nanoparticles is to increase the effectiveness of the treatment. Figure 1 shows a simplified version on the use of these radionuclides in the proposed treatment. On the left is the traditional radiopharmaceutical approach, where a radionuclide is attached to the targeting compound, which will then find its way to one of the cancer cells. It will then attach itself to the cell via a cancer-specific receptor before the treatment can begin. However, since the number of receptors are limited, there are only limited amount of radionuclides that can attach to the receptors. This limits the treatment dosage and depending on the stage of the cancer, may not be as useful to the patient.

On the right side of figure 1-1, is the proposed idea, in which the gold nanoparticles, acting as carrier, will bring the radionuclides to the vicinity of the cancer cells with the help of the targeting compounds. The limited number of receptors are not an important issue since the AuNP can hold several of these radionuclides, increasing the radiation dosage to the cancer cells. Additionally, other auxiliary drugs could be added onto the AuNPs to help with either the treatment or locating the AuNPs in the treatment process. The latter point can provide the medical personnel with information and/or confirmation that the treatment is proceeding as expected, which is non-existent in the radiopharmaceutical method.

Production of gold nanoparticles are varied depending on the size and shape, but in general, there are two types of production method: inorganic and organic [26-31]. However, both methodologies use $HClAu_4$ as the base material; the $HClAu_4$ is reduced which will aggregate the Au atoms in the solution. Once the AuNPs reach the desired size and shape, they will need to be stabilized to stop

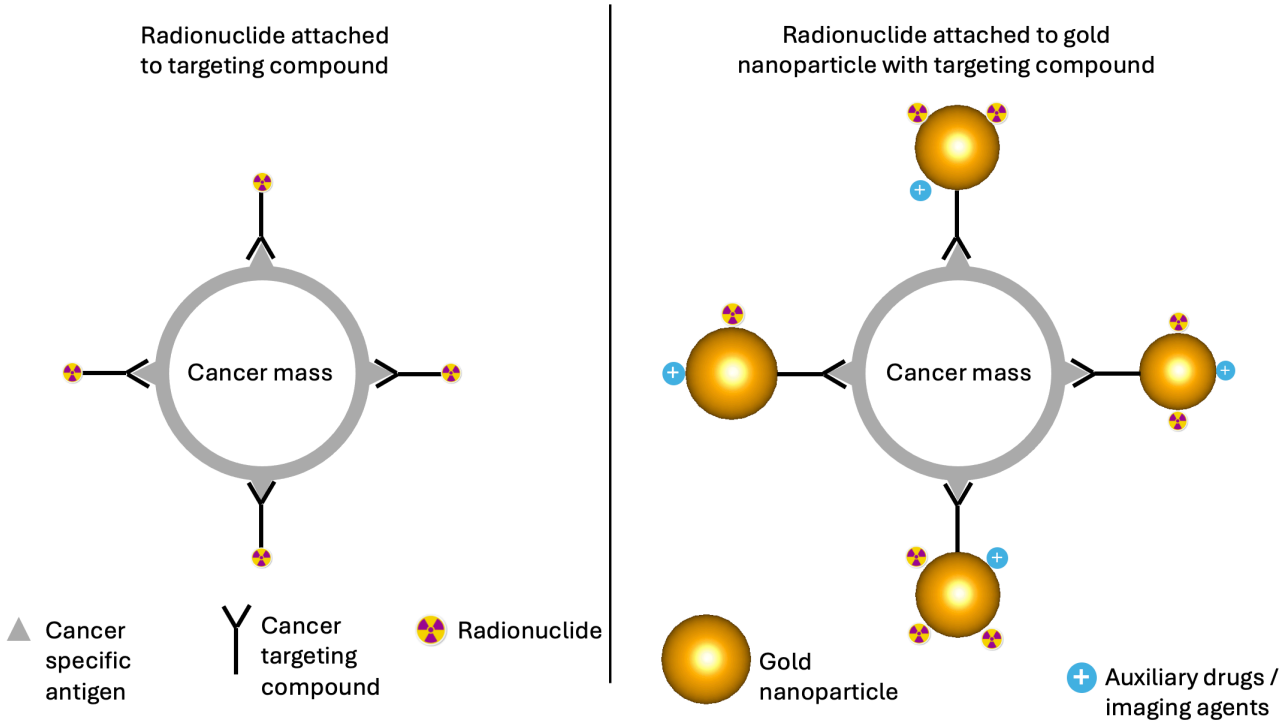

Figure 1-1. Schematics of TAT by radiopharmaceutical method of treatment (left) and carrier-utilization method (right) [25].

them from growing. They also need to be functionalized in order to allow biological components (e.g. the targeting compounds) to attach to the AuNPs. Usually, this function is performed by chemicals such as polyethylene glycol (PEG), which has the advantage of shielding the AuNPs from detection by the body's defensive mechanisms [32-33].

1.2 Objectives

Since this methodology is still relatively new, there are opportunities to improve on the knowledge of the fundamental science. By understanding the mechanism of adsorption between astatine and gold, we can provide physical justification on why gold is used. We can also learn some properties of astatine adsorption on gold by comparing it with a similar radionuclides. Additionally, adsorptions on stepped surface facets are studied to learn the adsorption strengths in such conditions. Once we know the science behind it can we propose a design to improve the current system.

The main objective of this study is to understand the bonding between gold (represented by gold slabs) and the halogen radionuclides (astatine and iodine). Additionally, the stability of adsorption should be confirmed for use in medical applications. Since the transport phase inside the body will take time, the adsorbates may desorb and potentially be absorbed by healthy organs which can be detrimental. With this information, we hope to provide the experimentalists and medical doctors the theoretical foundation to develop a more effective treatment for cancer.

1.3 Scope of this study

This study focuses on the adsorption astatine on gold surfaces as a representative for the more complex interactions that take place. It also covers the adsorption of iodine on gold surfaces as a comparison for astatine due to both elements being halogens. The configurations considered are only of gold and astatine or iodine, since the other additional molecules, such as drugs or targeting compounds, may vary. Additionally, only one atom of astatine or iodine will be studied at any one time. This allows the distances between the adsorbates to be large enough that no two adsorbates will be interacting with each other.

Since this study is designed to support the current initiative of the medical community, consideration of other metals are not included. While there may be other materials that can offer more advantages (cost, adsorption stability, or others), their use are still being investigated to ensure biocompatibility with the test subjects. Future works may look at expanding the studies into other metals that are being explored for use in the medical field.

Finally, this study will not cover the nuclear reactions that take place, both during production of the nuclear medicine or in its application.

References for chapter 1

[1] International Agency for Research on Cancer (2022, accessed 2024-06-22) .
[2] What is cancer - National Health Institute (accessed 2024-03-12) https://www.cancer.gov/about-cancer/understanding/what-is-cancer
[3] W. Link, Principles of Cancer Treatment and Anticancer Drug Development (Springer, 2019).
[4] J. E. Turner, Atoms, Radiation, and Radiation Protection (Wiley, 2007).
[5] P. Sigmund, Particle Penetration and Radiation Effects. General Aspects and Stopping of Swift Point Charges (Springer, 2006).
[6] Eds. P. Symonds, C. Deehan, J. A. Mills, C. Meredith, Walter and Miller's Textbook of Radiotherapy, Radiation Physics, Therapy and Oncology, 7th ed. (Elsevier, 2012).
[7] M. Yamamoto, Neurosurg. Clin. N. Am. 10 (1999) 181-202.
[8] S. Hertz and A. Roberts, J. Am. Med. Assoc. 131 (1946) 81-86.
[9] F. A. Mettler Jr. and M. J. Guiberteau, Essentials of Nuclear Medicine and Molecular Imaging, 7th ed. (Elsevier, Philadelphia, 2019).
[10] Q. Li, Y. Tian, D. Yang, Y. Liang, X. Cheng, and B. Gai, Tech. In Cancer Res. & Treatment 18 (2019) 1-8.
[11] S. Wei, C. Li, M. Li, Y. Xiong, Y. Jiang, H. Sun, B. Qiu, C. J. Lin, and J. Wang, Front. Oncology 11 (2021) 717180.
[12] C. Kratochwill, F. Bruchertseifer, F. L. Giesel, M. Weis, F. A. Verburg, F. Mottaghy, K. Kopka, C. Apostolidis, U. Haberkorn, and A. Morgenstern, J. Nucl. Med. 58 (2017) 1624-1631.
[13] Y. Dekempeneer, M. Keyaerts, A. Krasniqi, J. Puttemans, S. Muyldermans, T. Lahoutte, M. D'Huyvetter, and N. Devoogdt, Expert Opin. Biol. Therapy 16 (2016) 1035-1047.
[14] S. Poty, L. C. Francesconi, M. R. McDevitt, M. J. Morris, and J. S. Lewis, J. Nucl. Med. 59 (2018) 878-884.
[15] M. R. Zalutsky and M. Pruszynski, Curr. Radiopharm. 4 (2011) 177-185.
[16] G. Audi, O. Bersillon, J. Blachot, and A. H. Wapstra, Nucl. Phys. A 729 (2003) 3-128.
[17] B. Hammer and J. K. Nørskov, Nature 376 (1995) 238-240.
[18] R. Shukla, V. Bansai, M. Chaudhary, A. Basu, R. R. Bhonde, and M. Sastry, Langmuir 21 (2005) 10644-10654.
[19] M. Hu, J. Chen, Z-Y. Li, L. Au, G. V. Hartland, X. Li, M. Marquez and Y. Xia, Chem. Soc. Rev. 35 (2006) 1084-1094.
[20] S. A. Grant, C. S. Spradling, D. N. Grant, D. B. Fox, L. Jimenez, D. A. Grant, and R. J. Rone, J. Biomed. Mat. Res. A 102 (2016) 332-339.
[21] M. Kus-Liskiewicz, P. Fickers, and I. Ben Tahar, Int. J. Mol. Sci. 22 (2021) 10952.
[22] W. Cai, T. Gao, H. Hong, and J. Sun, Nanotechnol. Sci. Appl. 1 (208) 17-32.
[23] N. Daems, C. Michiels, S. Lucas, S. Baatout, and A. Aerts, Nucl. Med. Bio. 100-101 (2021) 61-90.
[24] F. Silva, M. P. Cabral Campello, and A. Paulo, Materials 14 (2021) 4.
[25] J. Tanudji, H. Kasai, M. Okada, T. Ogawa, S. M. Aspera, and H. Nakanishi, Phys. Chem. Chem. Phys. 26 (2024) 12915-12927.
[26] J. Turkevich, P. C. Stevenson, and J. Hillier, Discuss. Faraday Soc. 11 (1951) 55-75.
[27] G. Frens, Nature Phys. Sci. 241 (1973) 20-22.
[28] M. L. Machesky, W. O. Andrade, and A. W. Rose, Chem. Geol. 102 (1992) 53-71.
[29] M. Brust, M. Walker, D. Bethell, D. J. Schriffin, and R. Whyman, J. Chem. Soc., Chem. Commun. (1994) 801-802.
[30] M. Singh, R. Kalaivani, S. Manikandan, N. Sangeetha, A. K. Kumaraguru, Appl. Nanosci. 3 (2013) 145-151.

[31] S. Corra, U. Lewandowska, E. M. Benetti, and H. Wennemers, Angew. Chem. Int. Ed. 55 (2016) 8542-8545.
[32] A. L. Klibanov, K. Maruyama, V. P. Torchilin, and L. Huang, FEBS Lett. 268 (1990) 235-237.
[33] S. Chen, K. Yang, R. G. Tuguntaev, A. Mozhi, J. Zhang, P. C. Wang, and X.-J. Liang, Nanomedicine 12 (2016) 269-286.

Chapter 2

Astatine atom adsorption on Au(111)

The study of astatine's adsorption on gold is important to find out the adsorption characteristics before going on to more applicative aspects. As mentioned before, several works have shown that gold can adsorb astatine on its surface and keep them there until the delivery inside the test subjects. However, since this is a new field, we still have limited knowledge on their fundamental properties, such as adsorption characteristics, charge distribution upon adsorption, etc. Therefore, the first step is to simulate the adsorption of astatine on gold surface in order to learn how both elements are interacting, compare the theoretical results with experimental results, and get a general understanding of the adsorption process.

2.1 Adsorption energy and geometry

First-principles calculations are performed using density functional theory, as implemented in the Vienna Ab Initio Simulation Package (VASP) [1,2]. The details of the calculations are written in Appendix B. The choice of a surface slab as the basis of the calculation is taken from a study done to look at the limit of finite-size effect on adsorption [3]. The study found that for a nanoparticle of size above 2.7 nm, the adsorption on its surface can be approximated as adsorption on a slab surface. The justification is made that since some of the experimental works are using AuNPs of 5nm diameter size or larger, that this slab surface approximation works for modeling the adsorption of astatine on the AuNPs. The choice of Au(111) is based on the finding that the (111) surface offers the most stable configuration among other low Miller index surfaces [4,5].

The clean slab is shown in figure 2-1, with (a) as the top view and (b) as the side view. The top three layers are allowed to relax, given by the black lines numbered from 1 to 3, and the bottom two layers are kept static to simulate bulk conditions.

Table 2-1. Interlayer distances after relaxation calculation.

Interlayer distance changes	This work [6]	Literature [7]
Layer 1 to layer 2	2.1%	3.3 ± 0.4%
Layer 2 to layer 3	-0.7%	-0.8 ± 0.4%

Table 2-1 shows the result of the final relaxed geometry of the slab. The calculated values are consistent with the results obtained from the literature. With this, I continued my calculations to find out the most stable adsorption position for astatine on Au(111).

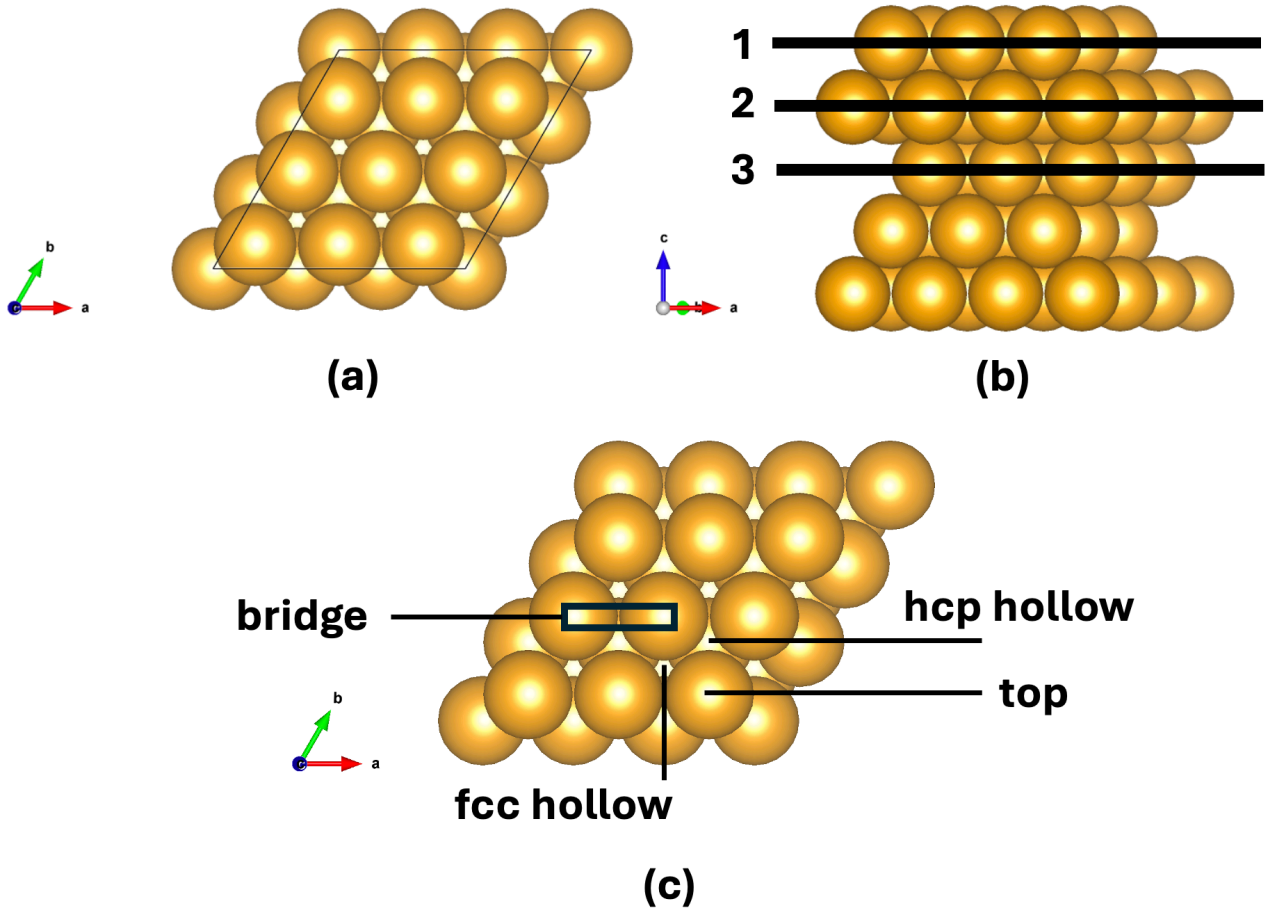

Figure 2-1. (a) Top view of Au(111), (b) side view of Au(111), (c) possible adsorption sites of Au(111).

The adsorption energies for astatine were calculated using the formula

$$E_{ad} = E_{At/Au(111)} - \left(0.5 \times E_{At_2} + E_{Au(111)}\right) \quad [1]$$

where E_{ad} represents the adsorption energy, $E_{At/Au(111)}$ represents the total energy of the At/Au(111) system, E_{At_2} represents the energy of the isolated At_2 dimer, and $E_{Au(111)}$ represents the total energy of the clean Au(111) slab.

Astatine does not exist in stable condition in standard temperature and pressure (STP) condition, and therefore, verification of the configuration of astatine has not been confirmed [8]. Therefore, following its categorization as halogen, the dimer At_2 is treated as being theoretically stable.

Table 2-2. Adsorption energy calculations for astatine on various adsorption sites of Au(111) [9,10].

Adsorption position	Energy (non-vdW) [eV]	Energy (vdW) [eV]	Energy (vdW + SOC) [eV]
bridge	-0.85	-1.37	-1.40
fcc-hollow	-0.91	-1.43	-1.43
hcp-hollow	-0.90	-1.42	-1.43
top	-0.59	-1.20	-1.26

Astatine was found to be most strongly adsorbed on the hollow sites: both fcc-hollow and hcp-hollow sites gave almost the same results. Therefore, I selected the fcc-hollow site as the primary adsorption site going forward since it is slightly stronger than the adsorption on the hcp-hollow site. At this point, a calculation choice is made between without van der Waals correction (non-vdW) or with van der Waals correction (vdW). The calculation results are written in table 2-1. Calculations including vdW yield a closer result to the experimental result, which was found to be approximately -1.6 eV [11]. Spin-orbit coupling (SOC) is another correction that is included due to the heavy nature of astatine. While SOC can appear in light elements, its presence is more pronounced in heavier elements. As can be seen from table 2-1, the difference in energies after considering SOC is very small, which means energetically, this correction is not that important compared to the vdW correction. Regardless, all the calculations yield the same trend: that hollow-sites are the most favorable adsorption positions.

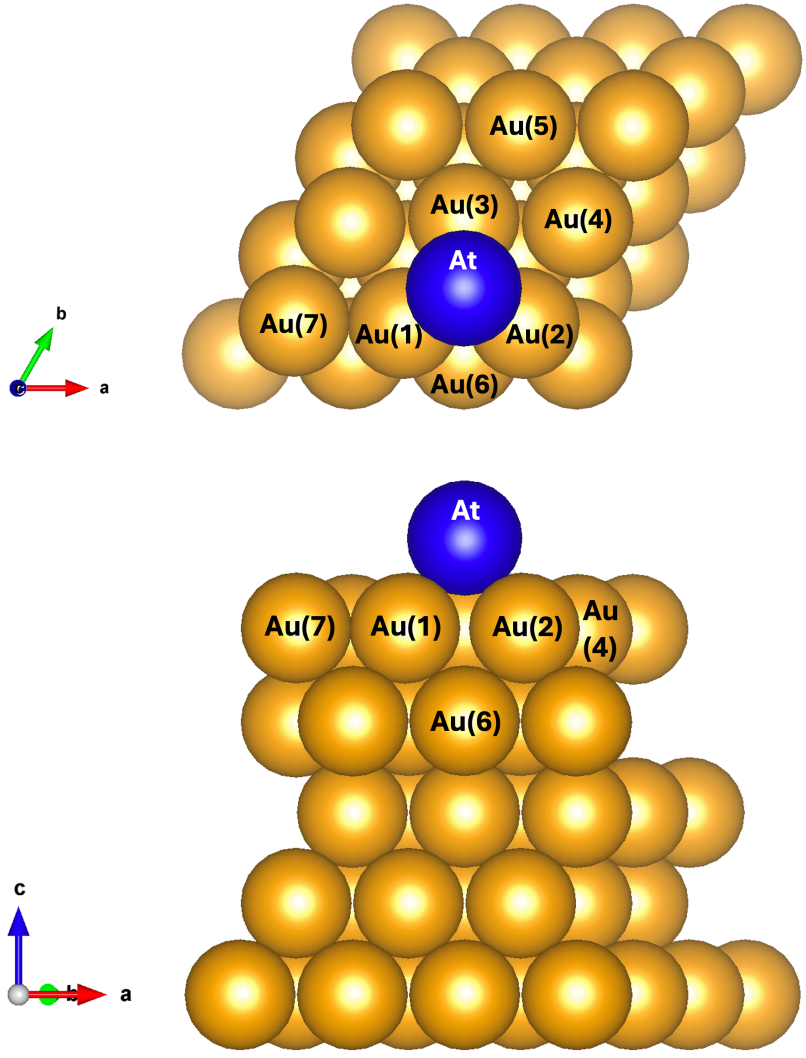

Figure 2-2. Top (above) and side (below) views of final adsorption configuration of At/Au(111).

Table 2-3. Distance between selected atoms of the At/Au(111) system.

Atoms	Distance (w/o vdW) [Å]	Distance (vdW) [Å]	Distance (vdW + SOC) [Å]
At - nearest Au atom	2.96	2.95	2.99
At - Au surface	2.34	2.35	2.42
Au(1) - Au(2)	3.14	3.10	3.06
Au(1) - Au(7)	2.85	2.82	2.82
Au(3) - Au(4)	2.98	2.93	2.92
Au(1) - Au(6)	2.99	2.96	2.95

Another effect of considering the SOC in calculations is in the different resultant geometry of interaction. There are works that predict reduction of bond length when including SOC, while others found the bond length to increase [12-14]. From figure 2-2 and table 2-3, I found the bonding distances between astatine and gold increases slightly due to considering SOC in the calculations. The effect of this increase on the adsorption energy however is not significant as shown in table 2-2.

2.2 Mechanism of adsorption

Based on the previous energy calculations, the adsorption mechanism was found to be chemisorption due to the strength of the bonding. Since any interaction between two particles requires the involvement of electrons, the bonding process can also be ascertained in more detail as ionic or covalent. To study further, we now look at the charge transfer as well as the densities of states.

The charge transfer can be quantified using Bader charge calculations. Since it assigns each charge to a particular atom, it is possible to determine which atom end up with more or less charge in its volume. Bader charges calculated before and after the bonding process reveal that the adsorption process is more covalent than ionic. For comparison, Bader charges for an ionic bonding and covalent bonding are also given, all shown in table 2-4. A positive value indicates the atom in question gains charge by that amount while a negative value indicates that atom loses charge by the indicated amount.

Table 2-4. Bader charge differences for At/Au(111) system compared to other types of compounds.

	Bader charge difference (vdW)	Bader charge difference (vdW+SOC)
Au in At/Au	0.00*e*	0.02*e*
At in At/Au	-0.02*e*	-0.09*e*
Na in NaCl	-0.86*e*	N/A
Cl in NaCl	0.86*e*	N/A
Cl in Cl_2	±0.04*e*	N/A

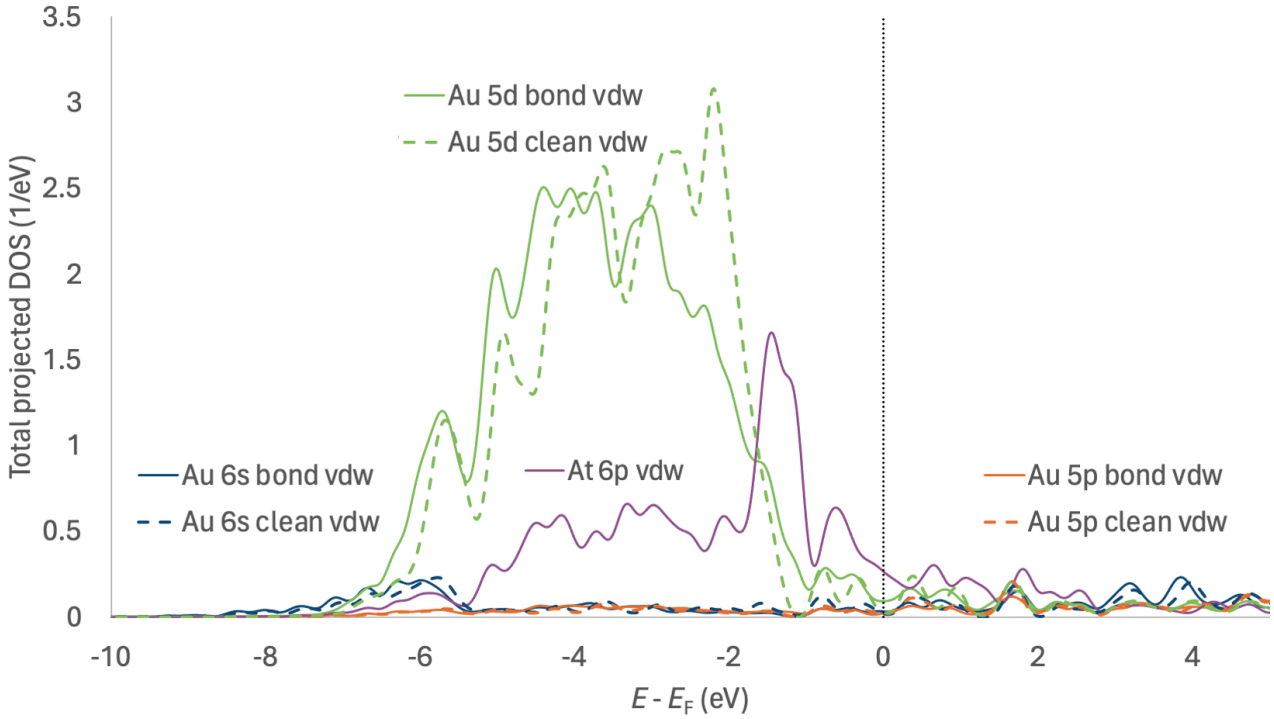

(a)

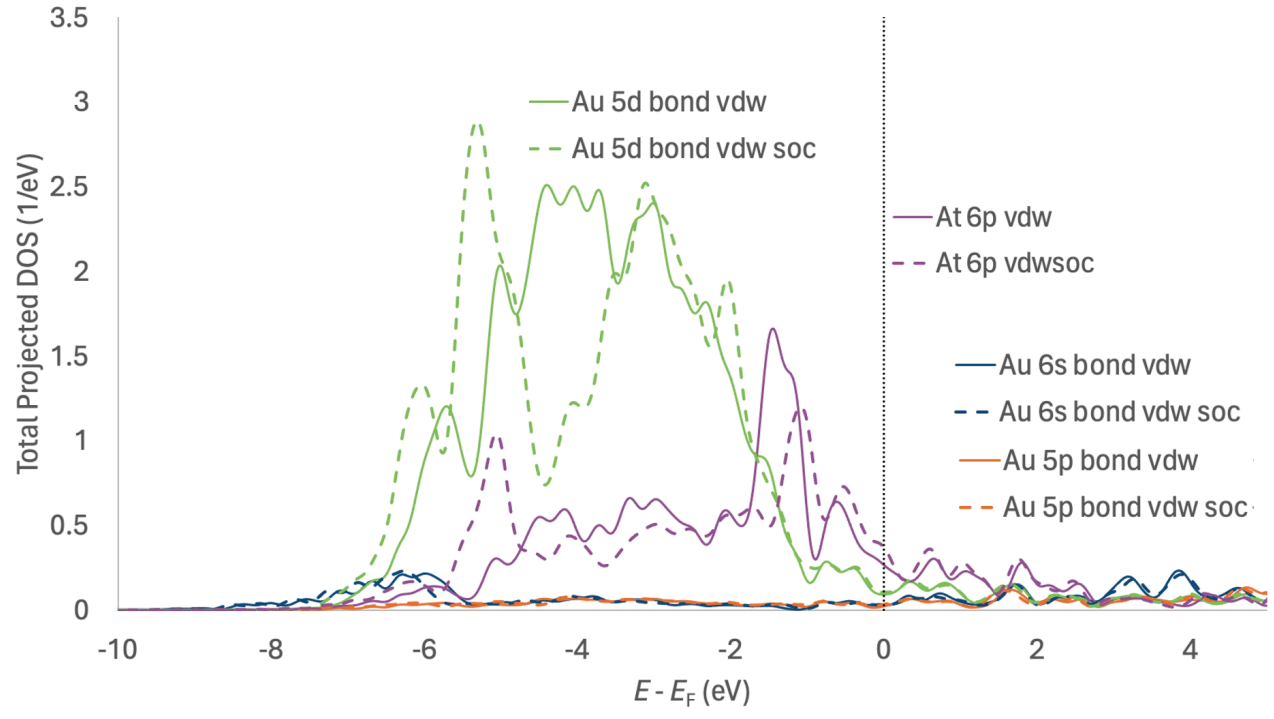

(b)

Figure 2-4. Comparison of densities of state of At/Au(111) system. (a) Before and after adsorption (considering vdW) (b) vdW and vdW + SOC.

There is only a limited charge movement between the astatine and gold, indicating that the electrons are shared between both reactants. We can see the bonding is much more similar to the covalent

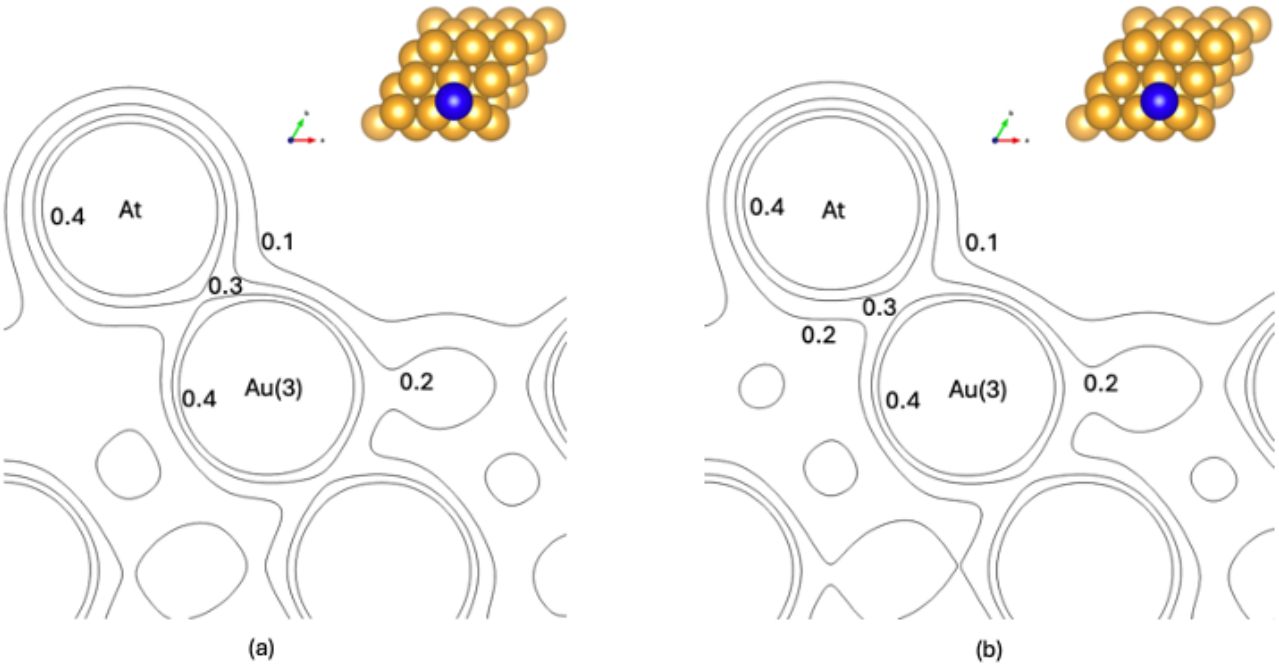

Figure 2-3. Charge contour plots of astatine on fcc-hollow site of Au(111), taken from the (210) plane. (a) With only vdW consideration (b) With vdW + SOC consideration.

bonding between Cl_2 than an ionic bonding experienced by NaCl. Astatine, although a halogen, is in this case being an electron donor to gold.

The charge contour plot shows charges accumulating in the middle of the astatine and gold atoms. Each contour line corresponds to a 0.1 $e\text{Å}^{-3}$ difference in charge density. Due to the symmetry of the adsorption, the charge contours for astatine on Au(1) and Au(2) is almost identical. This means that the charges shared by the three gold atoms are approximately a third of what the astatine lost. Since the gold atoms are in a slab configuration, the charge lost by astatine is distributed throughout the volume, although the bulk of the electron transfer are retained by the three surface atoms. Both contour plots show similar charge densities, with the (b) plot exhibiting less charge interaction between the astatine and the surface gold atom. This may be due to the slightly longer adsorption distance after considering SOC, but is not a large factor due to the adsorption energies being similar (table 2-2). In both cases, charge accumulation between the astatine and gold supports the argument the bonding between them is covalent, because a similar plot for NaCl would show almost no sharing of electrons between the Na and Cl atoms.

Two density of states plots are given for comparison purposes in figure 2-4. The vertical black dotted line represents the Fermi energy, and all readings are based from that reference line (negative and positive values correspond to occupied and unoccupied states, respectively). Figure 2-4a shows the effect of the adsorption of astatine on a clean surface of gold. Here, we can see the bonding of astatine affects the gold orbitals, namely the 5d and the 6s. Hybridization of the astatine 6p with the gold 5d and 6s orbitals can also be seen, especially around the -6 eV and from -4.5 eV to -2 eV.

Figure 2-4b shows the adsorbed system, with and without the consideration of SOC. The main difference between the two is the separation of the Au 5d and At 6p orbitals into two peaks, one of higher and one of lower energy regime. This split is due to the separation of the total angular

momentum (j) components of the higher orbitals [15]. For the Au 5d, the j splits to j = 1.5 and 2.5, while for the At 6p, the j splits to j = 0.5 and j = 1.5. This splitting causes both Au 5d and At 6p to separate into two peaks. From this separation, we can see that the lower energy peak of At 6p hybridizes with the lower energy, making a stronger case for the covalent bonding of astatine to the gold surface.

2.3 Conclusion for chapter 2

I showed that astatine is able to adsorb on Au(111) surface via covalent bonding. This can be seen from the lack of charge transfer as well as the hybridization of the astatine 6p orbital with the gold 5p and 6s orbitals. The effect of SOC, while important in analyzing the electronic states, does not provide significant impact on energy calculation and therefore may be neglected in calculating adsorption energies.

Reference for chapter 2

[1] G. Kresse and J. Furthmüller, Phys. Rev. B 54 (1996) 11169.
[2] G. Kresse and J. Furthmüller, Comput. Mater. Sci. 6, (1996) 15.
[3] J. Kleis, J. Greeley, N. A. Romero, V. A. Morozov, H. Falsig, A. H. Larsen, J. Lu, J. J. Mortensen, M. Dulak, K. S. Thygesen, J. K. Nørskov, and K. W. Jacobsen, Catal. Lett. 141 (2011) 1067-1071.
[4] G. Grochola, S. P. Russo, and I. K. Snook, J. Chem. Phys. 127 (2007) 224705.
[5] D. Holec, P. Dumitraschkewitz, D. Volath, and F. D. Fischer, Nanomaterials 10 (2020) 484.
[6] J. Tanudji, S. M. Aspera, H. Kasai, M. Okada, T. Ogawa, and H. Nakanishi, e-J. Surf. Sci. Nanotech. 22 (2023) 38-45.
[7] A. R. Sandy, S. G. J. Mochrie, D. M. Zehner, K. G. Huang, and D. Gibbs, Phys. Rev. B 43 (1991) 4667.
[8] D. R. Lide (Ed.), CRC Handbook of Chemistry and Physics, 86th ed. (Taylor and Francis Group, Florida, 2005) pp. 4-5.
[9] J. Tanudji, S. M. Aspera, H. Kasai, M. Okada, T. Ogawa, and H. Nakanishi, Phys. Sci. Int. J. 26 (2022) 1-10.
[10] J. Tanudji, S. M. Aspera, and H. Kasai, e-J. Surf. Sci. Nanotech. 21 (2023) 318-323.
[11] A. Serov, N. V. Aksenov, G. A. Bozhikov, R. Eichler, R. Dressler, V. Ya. Lebedev, O. Petrushkin, D. Piguet, S. Shishkin, E. Tereshatov, A. Türler, A. Vogele, D. Wittwer, and H. W. Gaggeler, Radiochim. Acta 99 (2011) 593-600.
[12] P. Pyykkö, Chem. Rev. 88 (1988) 563-594.
[13] P. Pyykkö, Angew. Chem., Int. Ed. 43 (2004) 4412-4456.
[14] E. Rossi, M. De Santis, D. Sorbelli, L. Storchi, L. Belpassi, and P. Belanzoni, Phys. Chem. Chem. Phys. 22 (2020) 1897-1910.
[15] N. E. Christensen, J. Phys. F 8 (1978) L51.

Chapter 3

Iodine atom adsorption on Au(111)

The findings on the previous chapter align with the experimental results that astatine on gold nanoparticles can be used to deliver targeted alpha therapy to cancer masses. Considering that this is a new methodology, I wanted to look at an already established radionuclide that could potentially be an alternative to TAT, i.e. iodine. Iodine has been used for thyroid cancer treatment since the 1940s, and there have been studies that explore other usage of iodine radioisotopes to enhance its flexibility [1-3]. The primary difference between astatine and iodine is in the decay product; whereas astatine releases an alpha particle, iodine releases beta and gamma radiations.

3.1 Adsorption energy and geometry

Table 3-1 Adsorption of a single iodine and single astatine on Au(111) [4].

Adsorption position	I/Au(111) Energy (w/o vdW) [eV]	I/Au(111) Energy (vdW) [eV]	I/Au(111) Energy (vdW +SOC) [eV]	At/Au(111) Energy (vdW) [eV]	At/Au(111) Energy (vdW + SOC) [eV]
bridge	-0.85	-1.29	-1.30	-1.37	-1.40
fcc hollow	-0.92	-1.33	-1.34	-1.43	-1.43
hcp hollow	-0.90	-1.33	-1.34	-1.42	-1.43
top	-0.62	-1.11	-1.14	-1.20	-1.26

Table 3-1 shows the adsorption energies of a single iodine atom on Au(111) surface, as well as a single astatine atom on Au(111) for comparison. As before, two sets of calculation, one considering SOC and another one that does not are performed. We can see minimal changes in the energy after SOC application, which is consistent with the finding in the previous chapter that SOC correction does not affect the adsorption energies significantly. The calculations also support the experimental finding that the labeling (i.e. adsorption) of iodine on gold nanoparticle is by chemisorption [5]. Similar to the At/Au(111) system, the addition of vdW has a much greater effect than SOC, although the trend for adsorption is the same with or without the corrections.

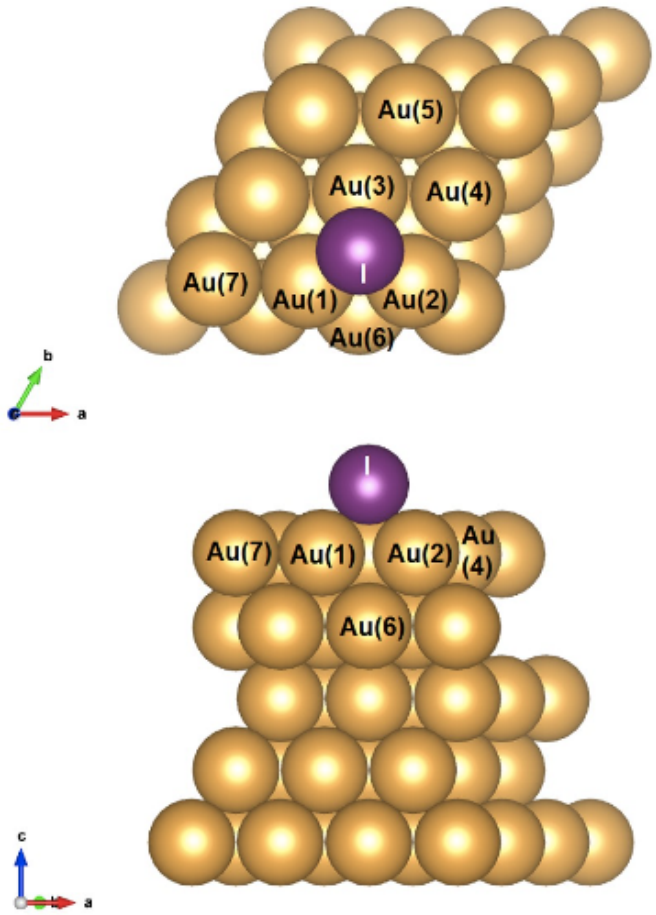

Figure 3-1. Top (above) and side views (below) of the final adsorption of iodine on Au(111).

Table 3-2. Distance between selected atoms of the I/Au(111) system.

Atoms	Distance (w/o vdW) [Å]	Distance (vdW) [Å]	Distance (vdW + SOC) [Å]
I - nearest Au atom	2.80	2.87	2.89
I - Au surface	2.23	2.25	2.28
Au(1) - Au(2)	3.16	3.11	3.07
Au(1) - Au(7)	2.85	2.82	2.81
Au(3) - Au(4)	2.98	2.94	2.92
Au(1) - Au(6)	3.00	2.97	2.96

The final configuration of the adsorption, shown in figure 3-1, is found to be at the fcc-hollow site, the same with At/Au(111). The 3 gold atoms surrounding the fcc-hollow has increased their distances from 2.91 Å, which is their initial interatomic distance, by an average of 0.2 Å to accommodate the incoming iodine atom. This further supports chemisorption being the adsorption mechanism, since physisorption will not be strong enough to cause a deformation on the slab surface.

3.2 Comparison with astatine

Before comparing the I/Au(111) system to At/Au(111) system, there is another interesting aspect that differentiates them, and that is the presence of electrons in the 4f orbital. Based on the Aufbau principle, the 4f orbital starts to be filled after the 6s orbital. This corresponds to one period lower from iodine, affecting Cerium and heavier elements. One of the effect of this filling is the decreased charge shielding offered by the 4f electrons, resulting in what has been termed "Lanthanoid contraction," named for the series that it first showed up [6,7]. The consequence of this phenomenon is the reduction of atomic radius for elements with higher atomic numbers [7,8]. This results in the adsorption distances of iodine on Au(111) to be very similar to that of astatine on Au(111) despite astatine being 1 period down from iodine.

When a comparison is made between the final configuration of I/Au(111) with At/Au(111), the results gives similar values. While this may be expected since both iodine and astatine is adsorbed on the same surface facet, it shows a similar phenomenon happening in the At/Au(111) case. The gold surface atoms moved by almost the same amount for At/Au(111) as they did for I/Au(111). This indicates there is a limit on the ability of the gold atoms to move due to the packing structure of the (111) surface. Therefore the two adsorbates, being almost equal in size with a gold atom, can

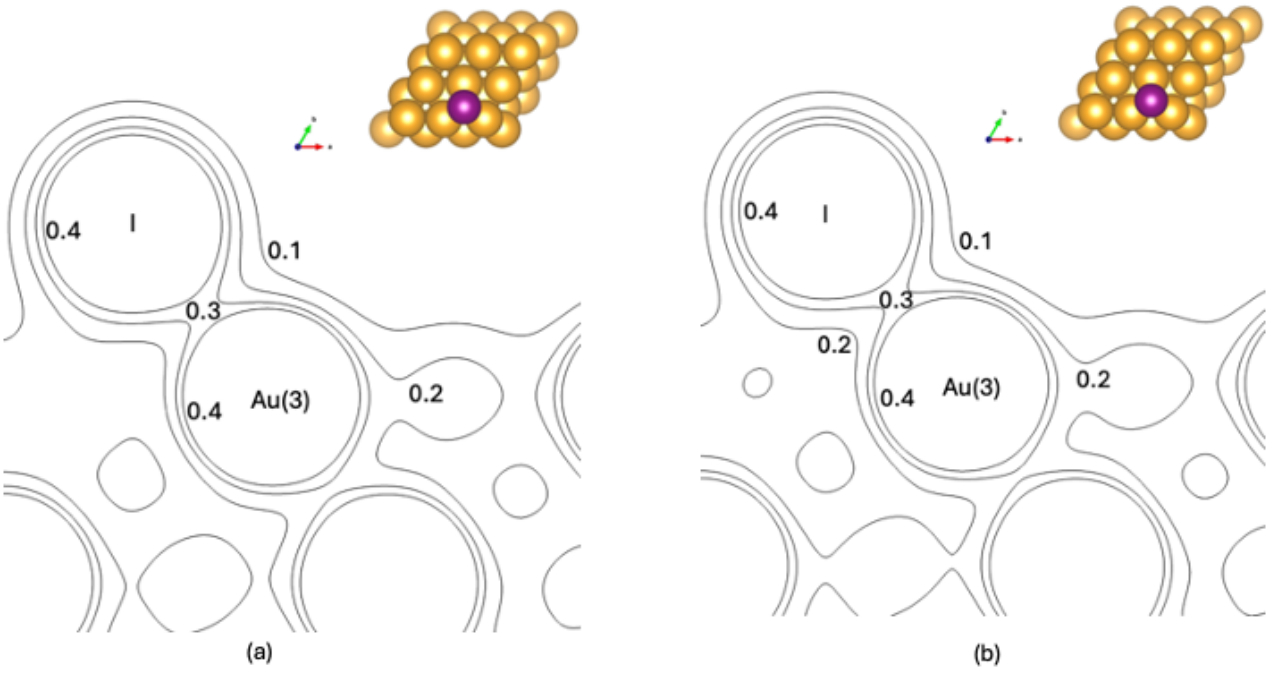

Figure 3-2. Charge contour plots of iodine on fcc-hollow site of Au(111), taken from the (210) plane. (a) Plot with vdW consideration (b) Plot with vdW + SOC consideration.

only stay at some distance away, which may explain why smaller radius halogens have stronger bonding to gold surface. This, however, is not true in astatine's case. Even though the adsorption distance is longer than iodine, the adsorption energy of astatine on gold is still slightly stronger. This could be due to the lanthanide contraction and the poor shielding offered by the electrons in the 4f orbital, which caused the nucleus to have a stronger effect in the bonding process.

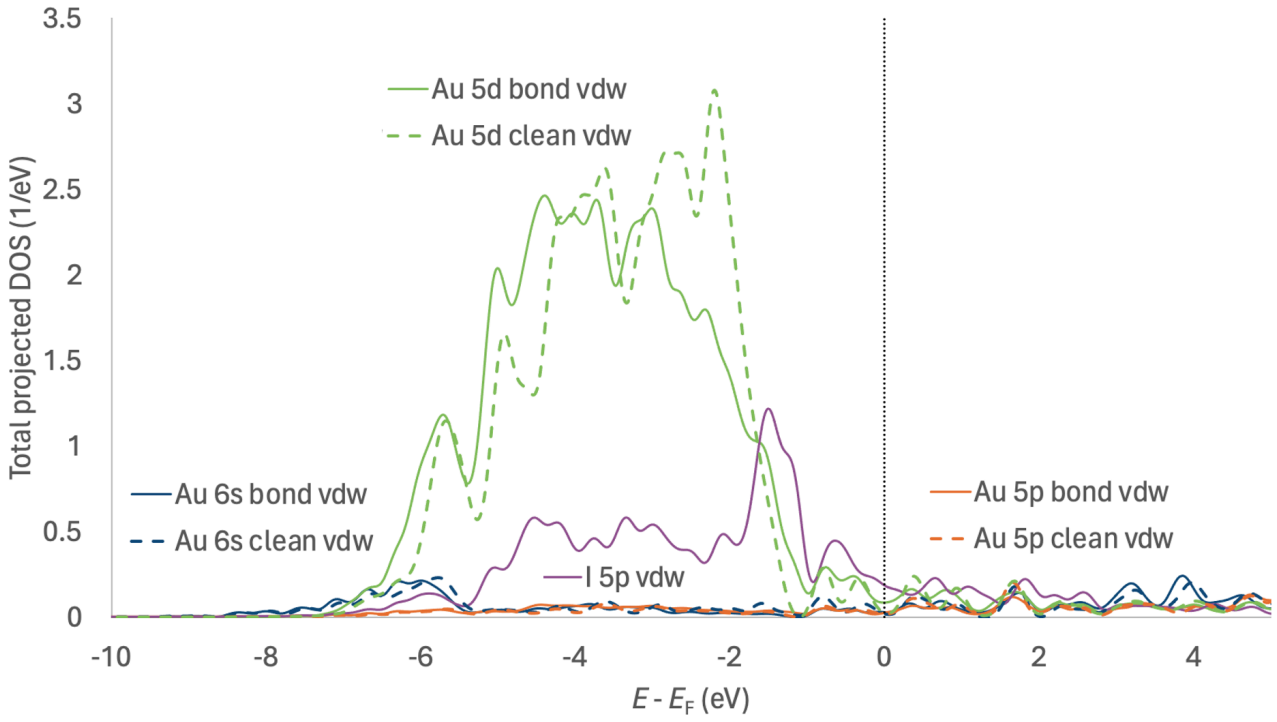

(a)

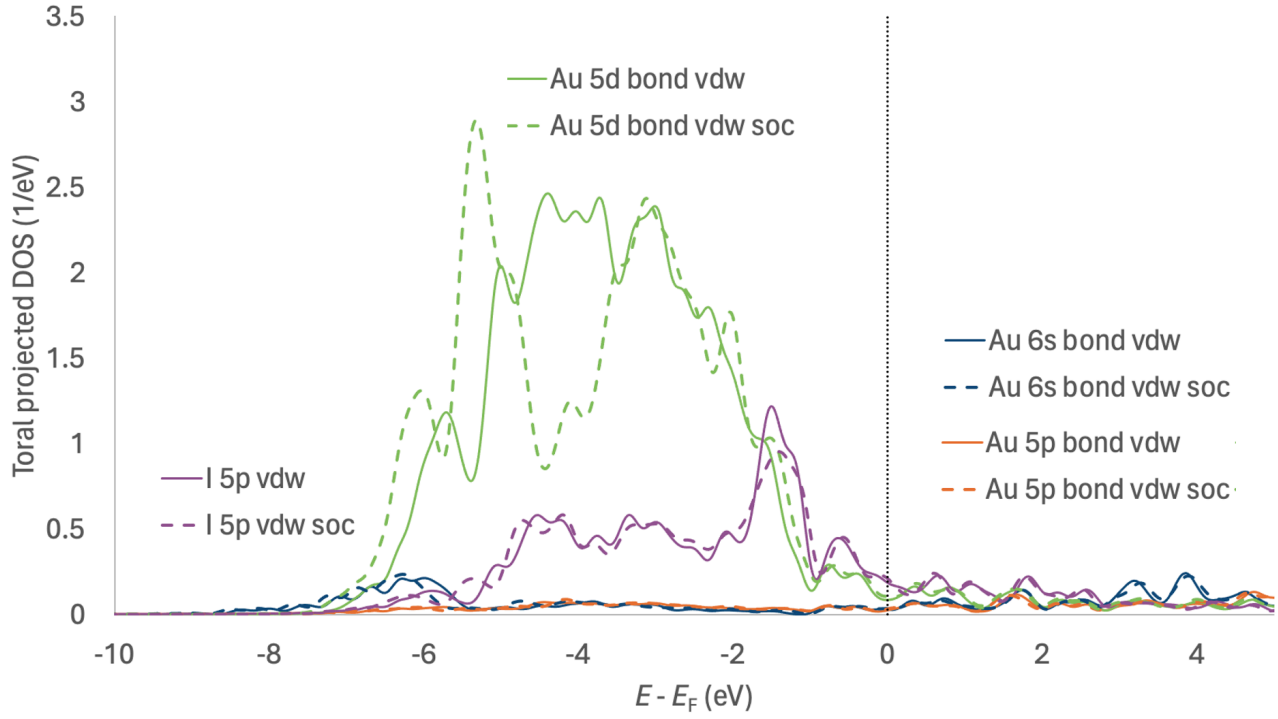

(b)

Figure 3-3. Comparison of densities of state of I/Au(111) system. (a) Before and after adsorption (considering vdW) (b) vdW and vdW + SOC.

Charge contour plots of I/Au(111) system with and without SOC consideration are shown in figure 3-2. We can see that the charge contours are mostly the same, due to the similarity of the bonding distances. This implies that SOC consideration has almost no effect on the charge transfers of the system as a whole. Another point to discuss is the charge contours are mostly affected by the

adsorption distance of the adsorbate and the surface. The comparison to figure 2-3 shows that due to the increase in adsorption distance with SOC consideration, the charge concentration between astatine and gold decreased slightly.

Table 3-3. Bader charge differences for I/Au(111) and At/Au(111) systems.

	Bader charge difference (vdW)	Bader charge difference (vdW+SOC)
Au in I/Au	-0.02*e*	-0.03*e*
I in I/Au	0.08*e*	0.07*e*
Au in At/Au	0.00*e*	0.02*e*
At in At/Au	-0.02*e*	-0.09*e*

Looking at table 3-3, the similarities of the amounts indicate that iodine adsorbs on the gold surface via covalent bonding, with a tendency to be a charge recipient. In comparison to astatine, which stayed either constant or slightly positive, iodine tends to receive charges from the gold atoms, albeit in a very small amount. The tendency for iodine to assume a negative charge can be explained by it being a halogen, which typically would accept one electron in order to complete its valence shell. This can be seen in table 2-4, where chlorine in NaCl accepts 0.86 charges in the process of bonding. Since iodine binds covalently with gold, such large charge movements are absent.

In figure 3-3, the comparison between densities of state before and after adsorption is shown in the top part. Similar to the conclusion obtained in the previous section, iodine adsorbs on gold by covalent bonding, with the same energy ranges that show hybridization between iodine 5p and gold 5d and 6s orbitals. The difference is when the DOS for calculations involving SOC is plotted. There is no splitting for the iodine 5p orbital and the shape is generally similar to the calculations without SOC consideration. This also indicates that iodine is not affected by SOC.

3.3 Conclusion for Chapter 3

The adsorption of iodine on Au(111) provides an interesting comparison to astatine since both are halogens and both are important sources of radiation for radiotherapy purposes. Due to both elements being classified as halogens, similar characteristics can be observed in the adsorption process. Both iodine and astatine adsorb on Au(111) by covalent bonding, with hybridization of the halogens' p orbitals with gold 5d and 6s orbitals. Astatine's adsorption energy was found to be slightly stronger than iodine, which is useful for its application for radiotherapy.

References for chapter 3

[1] S. C. Werner, E. H. Quimby, and C. Schmidt, Am. J. Med. 7 (1949) 731-740.
[2] Q. Li, Y. Tian, D. Yang, Y. Liang, X. Cheng, and B. Gai, Tech. In Cancer Res. & Treatment 18 (2019) 1-8.
[3] S. Wei, C. Li, M. Li, Y. Xiong, Y. Jiang, H. Sun, B. Qiu, C. J. Lin, and J. Wang, Front. Oncology 11 (2021) 717180.
[4] J. Tanudji, S. M. Aspera, and H. Kasai, e-J. Surf. Sci. Nanotech. 21 (2023) 318-323.
[5] A. A. Walsh, J. Nanopart. Res. 19 (2017) 152.
[6] P. Pyykkö, Chem. Rev. 88 (1988) 563-594.
[6] V. M. Goldschmidt and T. F. W. Barth, “Geochemische Verteilungsgesetze der Elemente 5,” Ja. Dybwad, Oslo (1925).
[7] R. Shannon, Acta Cryst. A 32 (1976) 751.
[8] M. Alaydrus, M. Sakaue, and H. Kasai, Phys. Chem. Chem. Phys. 18 (2016) 12938-12946.

Chapter 4

Adsorption of astatine or iodine on Au(211)

Theoretical simulation can construct precise surface facets as well as controlling certain variables such as the amount of adsorbates or surface defects, which allows for a more detailed study. However, in real life, things are not so simple. Gold nanoparticles are three dimensional structures; it is inherent for them to have different shapes and sizes, including different faces on the surface. The effect of surface facet therefore is important in understanding where adsorbates such as astatine or iodine may prefer to be adsorbed.

4.1 Energy and geometry of astatine or iodine adsorption on Au(211)

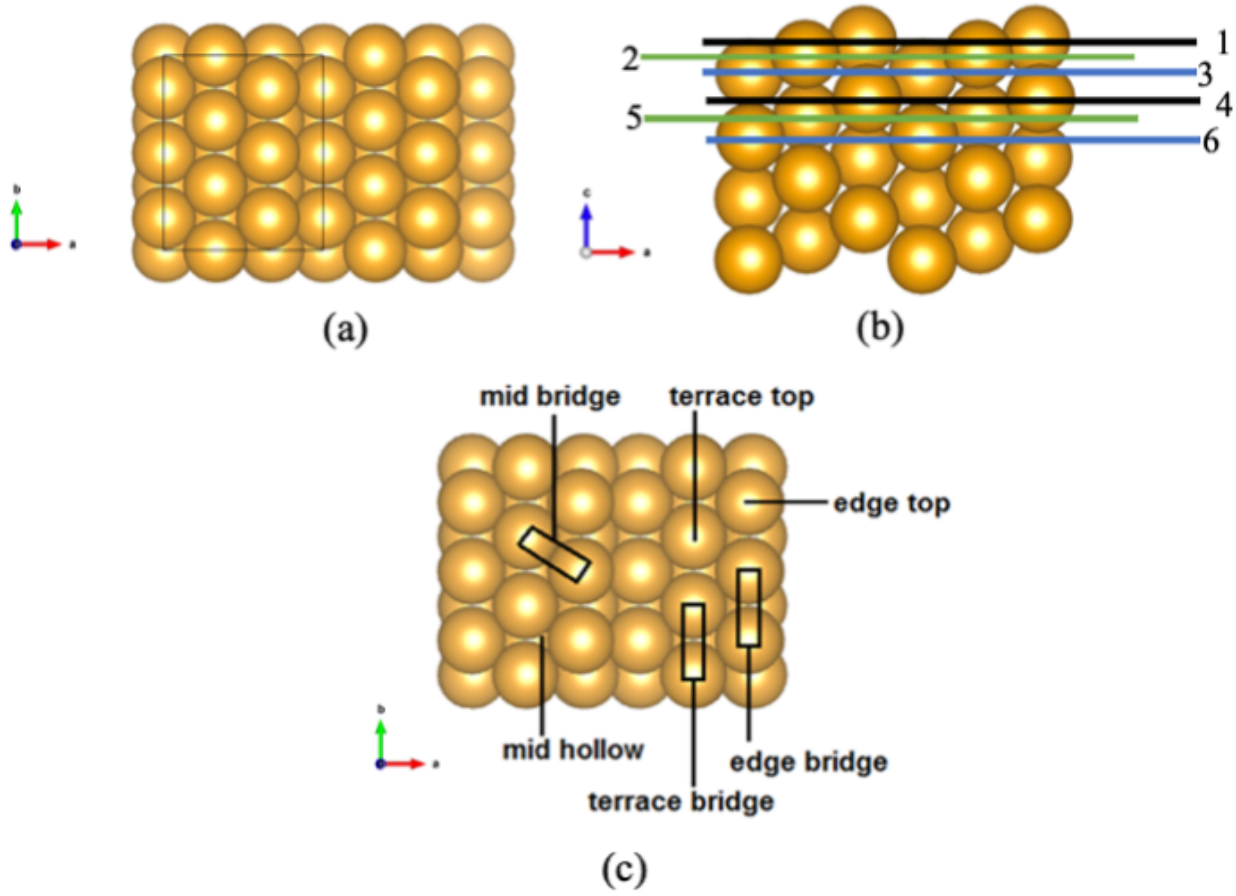

Figure 4-1. (a) Top view of Au(111), (b) side view of Au(111), (c) possible adsorption sites of Au(111).

The previous study on astatine or iodine adsorption is based on a flat surface, based on the understanding that if Au(111) can adsorb them, more reactive surface facets can too. To learn more about the adsorption characteristics, I looked into the adsorption of astatine or iodine on a stepped

surface. This will provide a numerical comparison between a flat and stepped surface, as well as see the changes present in such adsorption cases.

In figure 4-1, the different views of Au(211) surface slab that will be used in these calculations, along with the possible adsorption sites listed. The slab shown is made of a 2x1 supercell of 2x3x6 gold atoms in order to highlight the stepped surface. These sites are designated slightly differently due to the presence of an edge that stops the Au(111) facet from continuing. The top half of the slab (layers 1 to 6 in figure 4-1 b) is allowed to relax while the bottom half is kept static to simulate bulk conditions.

A comparison of the relaxed layers can be made with the literature to determine the amount of contraction or expansion that took place in the slab during relaxation. The edge layer (layer 1 to layer 2) contracted, around -30%, compared to the literature's -4.2% [1,2]. One reason might be due to the limited layers that this work employed: since adsorption process is mostly a surface phenomenon, the simulation focuses mostly on the surface layers. The literature had much thicker slab while this work has a limited amount; this means that a small deviation in the c-direction will have a bigger impact on the percentage value. However, if one considers the interlayer difference, such as from layer 1 to layer 4, the contraction is calculated to be -4.5%, which is similar to the value given above.

Similar to the previous equations, the adsorption energies of the various systems can be calculated using the formula

$$E_{\text{ad}} = E_{\text{M/Au(X)}} - \left(0.5 \times E_{\text{M}_2} + E_{\text{Au(X)}}\right) \quad [2]$$

with the subscripts M and X representing an adsorbate (iodine or astatine) and the surface facet (111 or 211), respectively. E_{ad} represents the adsorption energy, $E_{\text{M/Au(X)}}$ represents the total energy of the adsorbate M on Au(X) system, E_{M_2} represents the energy of the isolated diatomic molecule of M, and $E_{\text{Au(X)}}$ represents the total energy of the clean Au(X) slab. The results are collated in table 4-1.

Table 4-1. Adsorption energies of astatine or iodine on Au(211) [1]

	Iodine		Astatine	
	Energy (vdW) [eV]	Energy (vdW + SOC) [eV]	Energy (vdW) [eV]	Energy (vdW + SOC) [eV]
Edge-bridge	-1.63	-1.64	-1.63	-1.61
Edge-top	-1.18	-1.21	-1.19	-1.24
Mid-hollow	-1.38	-1.37	-1.47	-1.45
Terrace-top	-1.12	-1.13	-1.22	-1.27

The final configuration of astatine on Au(211) can be seen in figure 4-2 and its adsorption geometry is given in table 4-2. For comparison, the geometry results of adsorption on Au(111) are given.

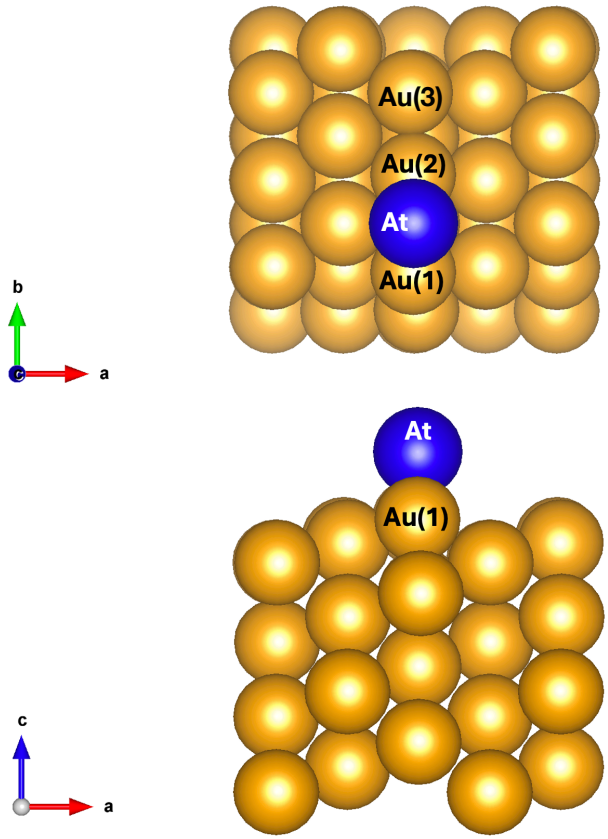

Figure 4-2. Top (above) and side views (below) of final adsorption of astatine on Au(211). The Au(211) slab is extended to show the stepped nature of the slab.

Table 4-2. Final distances of iodine or astatine on different gold surfaces [1,3].

	Iodine		Astatine	
	vdW [Å]	vdW + SOC [Å]	vdW [Å]	vdW + SOC [Å]
M - Au(211)	2.13	2.17	2.26	2.31
Au(211)_1 - Au(211)_2	3.26	3.22	3.25	3.21
Au(211)_2 - Au(211)_3	2.74	2.74	2.75	2.74
M - Au(111)	2.26	2.28	2.35	2.42
Au(111)_1 - Au(111)_2				
Au(111)_2 - Au(111)_3	3.11	3.07	3.10	3.06
Au(111)_1 - Au(111)_3				

4.2 Comparison between adsorption on stepped and flat surface

4.2.1 Adsorption configuration

The adsorption energy for a single iodine or astatine atom on Au(211) is stronger than the corresponding adsorption on Au(111). This is due to the more active edge site, as exemplified by the work function of the different surface facets. The calculated work function for Au(111) is 5.2 eV whereas it is 5.1 eV for Au(211). A smaller work function value indicates less energy is needed to remove an electron from the surface of the metal, which makes Au(211) to be more active than Au(111).

Another point is the similarity between the adsorption sites on the "flat" side of Au(211): the mid-hollow and terrace-top. The adsorption energy of the mid-hollow site closely resembles the adsorption energy of the hollow site of Au(111). Similarly the Au(211) terrace-top site mimics the Au(111) top site energetically. These reasons make the Au(211) to be a good contrast to Au(111), as the Au(111) surface can still be found in parts of Au(211).

From table 4-2, we see that both adsorbates end up closer to the surface of Au(211) than Au(111). This could be due to the relatively loose atomic layout in the a-b plane. Since the edge gold atoms have only the gold atoms on the terrace to hinder their movement, they are able to move more freely to accommodate the adsorbate. This causes the distance between Au(211)_2 and Au(211)_3 to decrease more than the bulk interatomic distance of ~2.9 Å. This squeeze allows for a larger space to open up for the astatine or iodine, and making them adsorb closer to the gold surface. This could not happen in a pristine Au(111) simply due to the closely-packed structure on the surface, as mentioned in earlier chapters.

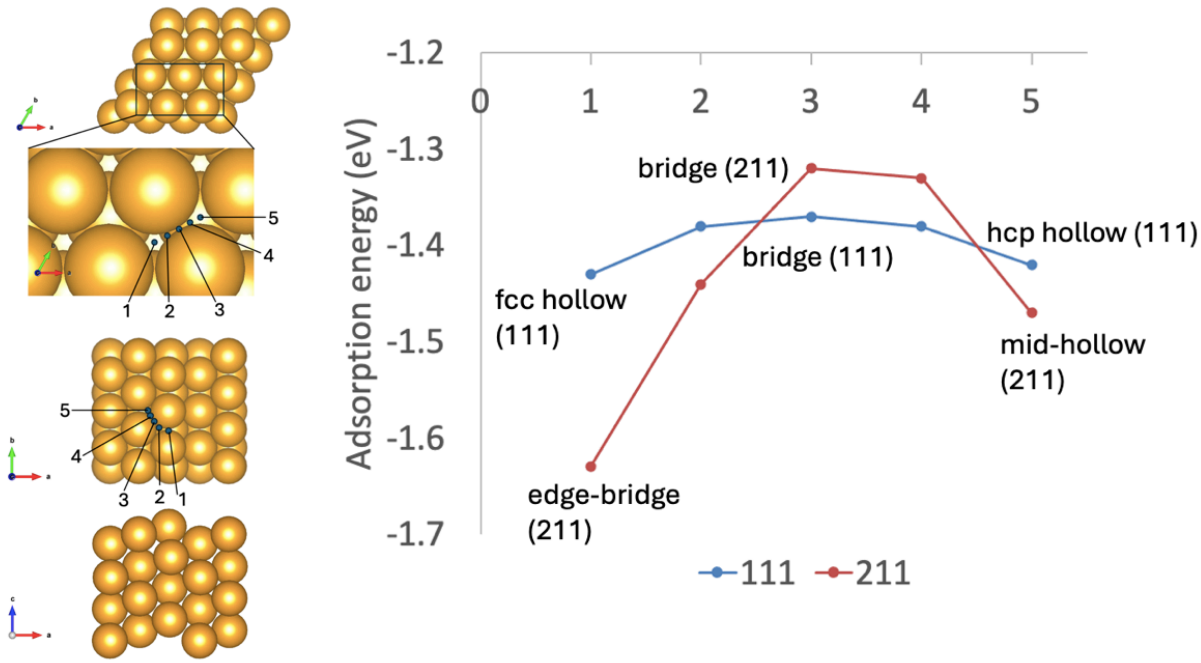

Figure 4-3. (Left) Astatine diffusion from the most stable site (1) to the second most stable site (5) for Au(111) (top) and Au(211) (bottom). (Right) the energy plots associated with the movement.

4.2.2 Stability of adsorbate

Having data for two different surfaces allow for comparison between the stability of adsorbates already on the surface. The idea is if the surface allows for easy movement on its surface, any external influence such as temperature may affect the behavior of the adsorbate, e.g. by moving around. This could potentially affect other adsorption taking place on the surface since the interaction between the present adsorbate and the incoming adsorbate may limit the amount of adsorbates present on the surface. For this calculation, I designated the point 1 as the most favorable adsorption site on that particular surface and point 5 as the second most favorable adsorption site (figure 4-3 left panel). In the Au(111) case, this means going from the fcc-hollow to the hcp-hollow, with a distance of 1.68 Å. For Au(211), the adsorbate goes from the edge-bridge site to the mid-hollow site, a distance of 2.54 Å. Since diffusion may take different paths, the path selected here is a shortest-distance case based on the previous distance values. Energy needed to overcome the barrier between the sites would determine how stable an adsorption position is.

From the right panel of figure 4-3, we find the Au(211) has a higher energy barrier than Au(111), at -0.31 eV compared to -0.08 eV. In both cases, this is due to the need for astatine to traverse between the two gold atoms before reaching its new placement. This bridge site is a less favorable place for astatine to adsorb, and so a lower adsorption energy is obtained. This energy difference effectively becomes the energy barrier that astatine has to overcome. Due to the symmetry of the Au(111), astatine going from point 5 to point 1 faces the same energy barrier, while in the case of Au(211), the energy barrier is lower, at 0.15 eV. This is still almost twice as much as the energy barrier for Au(111), making Au(211) a much more stable platform to adsorb and hold astatine.

4.2.3 Charges and densities of states

To investigate the bonding in more detail, the electronic states are studied, first by looking at the charge transfer for both surfaces.

Table 4-3. Bader charge differences for I/Au(211) and At/Au(211) systems.

	Iodine		Astatine	
	vdW	vdW + SOC	vdW	vdW + SOC
M in M/Au(211)	0.08*e*	0.06*e*	-0.01*e*	-0.08*e*
Au in M/Au(211)	0.01*e*	0.01*e*	0.04*e*	0.06*e*
M in M/Au(111)	0.08*e*	0.07*e*	-0.02*e*	-0.09*e*
Au in M/Au(111)	-0.02*e*	-0.03*e*	0.00*e*	0.02*e*

Comparing the Bader charges between the M/Au(211) system and the M/Au(111) system (table 4-3), there is not much difference in the charge movements for the adsorbates' cases. This strengthens the argument that the bonding between astatine or iodine on gold is covalent in nature, and that the electrons responsible for bonding are mostly shared between the affected atoms.

The contour plots in figure 4-4 show an increase in overlapping charges between the adsorbates and gold edge atoms. This is due to the charges being concentrated on two gold atoms instead of three. Additionally, the shorter adsorption distances mean that the charges are more concentrated in the spaces between astatine or iodine and the gold atoms. This is also reflected in the At/Au(211)

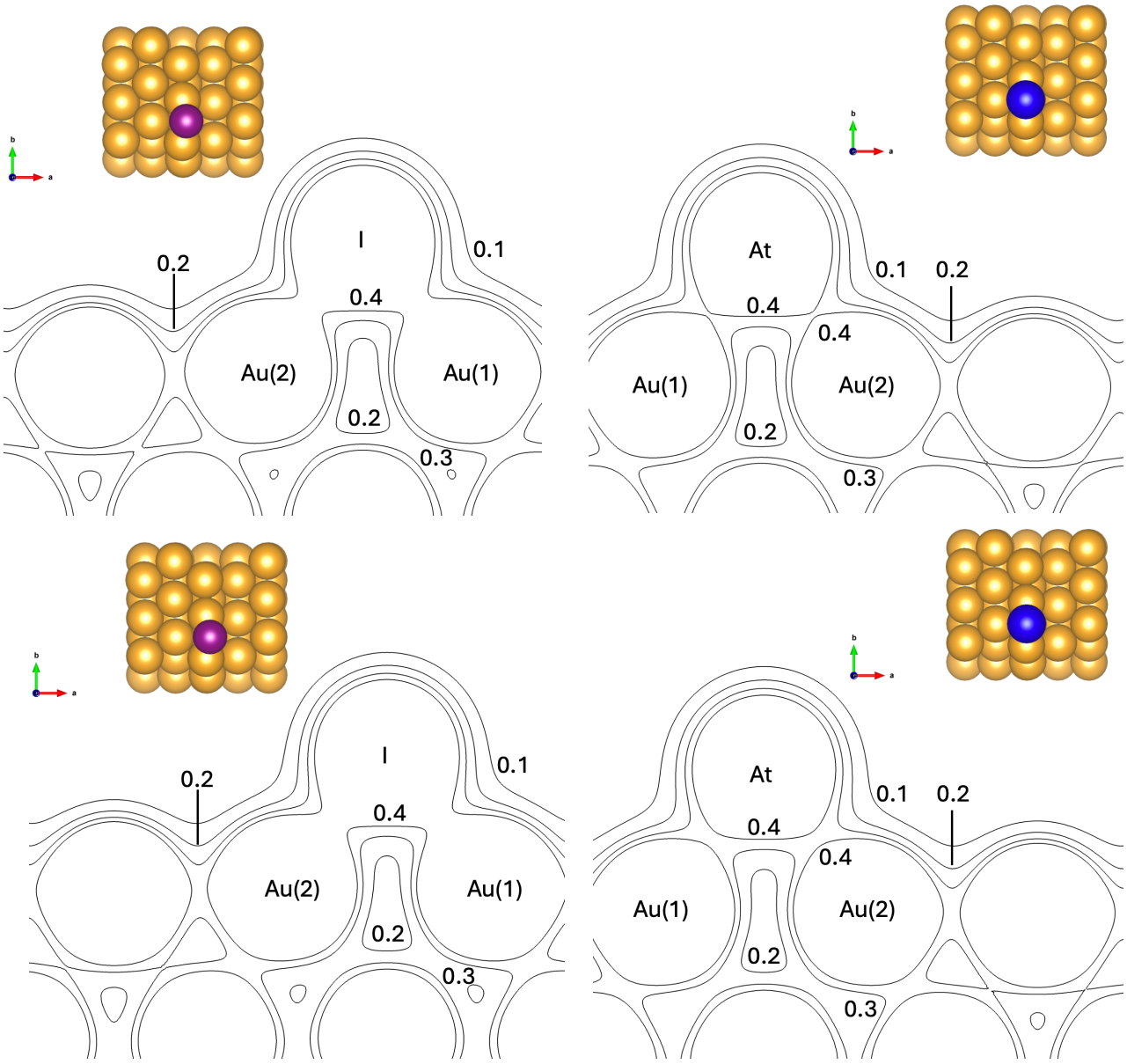

Figure 4-4. Contour plots of (top left) I/Au(211) with vdW, (top right) At/Au(211) with vdW, (bottom left) I/Au(211) with vdW + SOC, and (bottom right) At/Au(211) with vdW + SOC.

system where, due to the slightly longer adsorption distance, the charge contour overlap is not as large as I/At(211).

Finally, we look at the density of states of the M/Au(211) systems in figure 4-5. Both p orbitals of iodine and astatine produce similar effects after bonding. The 5d orbital of gold initially had a quantity of states around the -2 eV region, which were then reduced after bonding. These imply that the adsorption process makes the gold more stable, which can be seen with the overlap of the adsorbate's p orbital and the gold's 5d and 6s orbitals. The energy ranges for these hybridization remains the same: between -4.5 eV to -2 eV for the hybridization with the gold 5d and around -6 eV for the hybridization with the gold 6s.

The comparison between adsorption of astatine on flat and stepped surface can be seen in figure 4-6. In general, the peaks of astatine 6p correspond with each other, whether it is adsorbed on Au(111) or Au(211), which indicates that the hybridization between astatine and gold is similar across different surfaces. These however do not explain why the adsorption energies are 0.2 eV

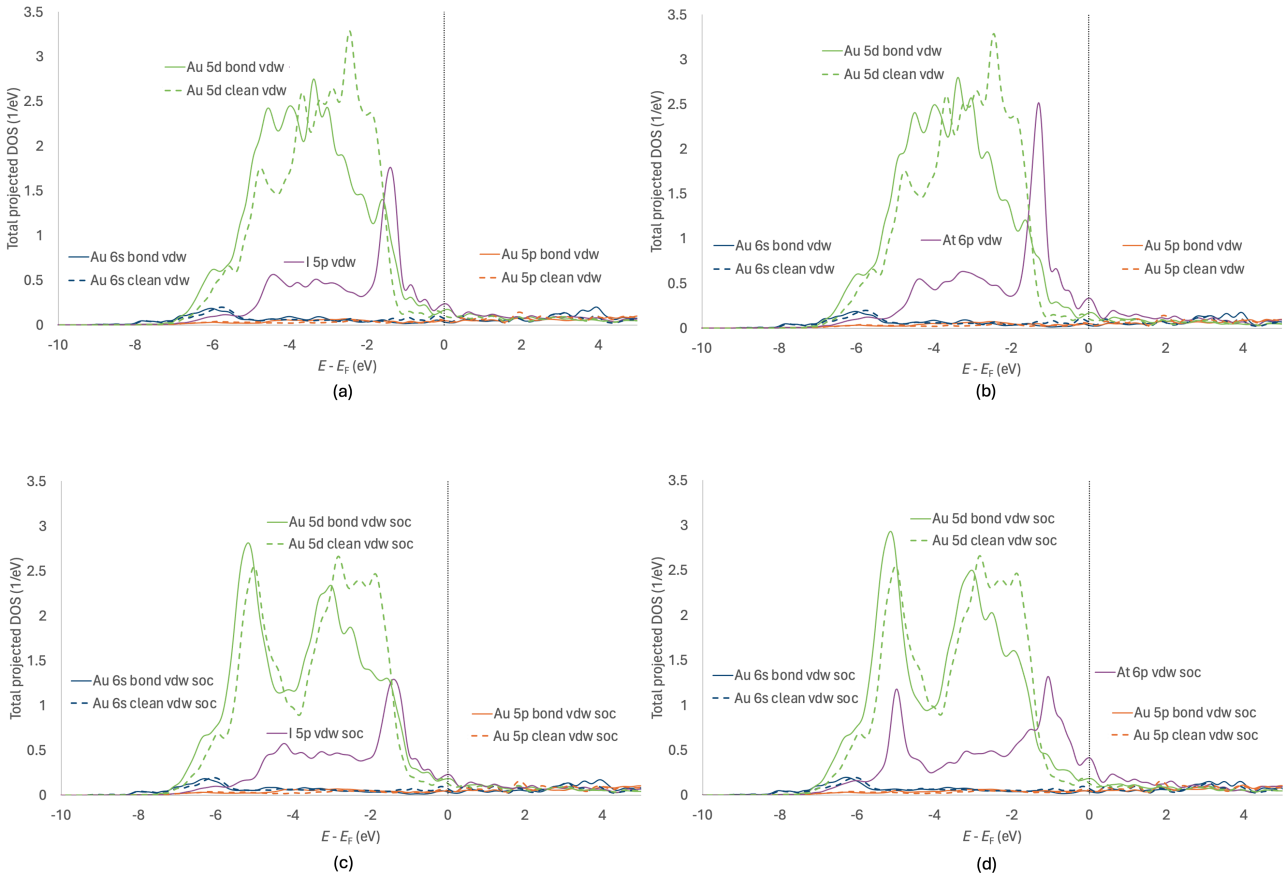

Figure 4-5. Comparison of densities of state before and after adsorption for (a) I/Au(211) with vdW, (b) At/Au(211) with vdW, (c) I/Au(211 with vdW and SOC, and (d) At/Au(211) with vdW and SOC.

stronger for the stepped case than the flat case. Since the Bader charge difference also gave similar results, the stronger adsorption must therefore be a property of the nature of the stepped surface, as indicated by the work function difference.

These results suggest that the surface of a constructed nanoparticle should be composed of more stepped or corrugated surfaces to allow for stronger adsorption of either astatine or iodine for treatment. Not only does Au(211) show superior adsorption capability compared to a flat Au(111), it is also able to keep the adsorbate stable on the adsorption site. Additionally, a three-dimensional nanoparticle will undoubtedly have some stepped edges as the curvature of the particle wraps around to form their shape. Making their diameters smaller will produce more of these jagged edges than a larger-sized nanoparticle.

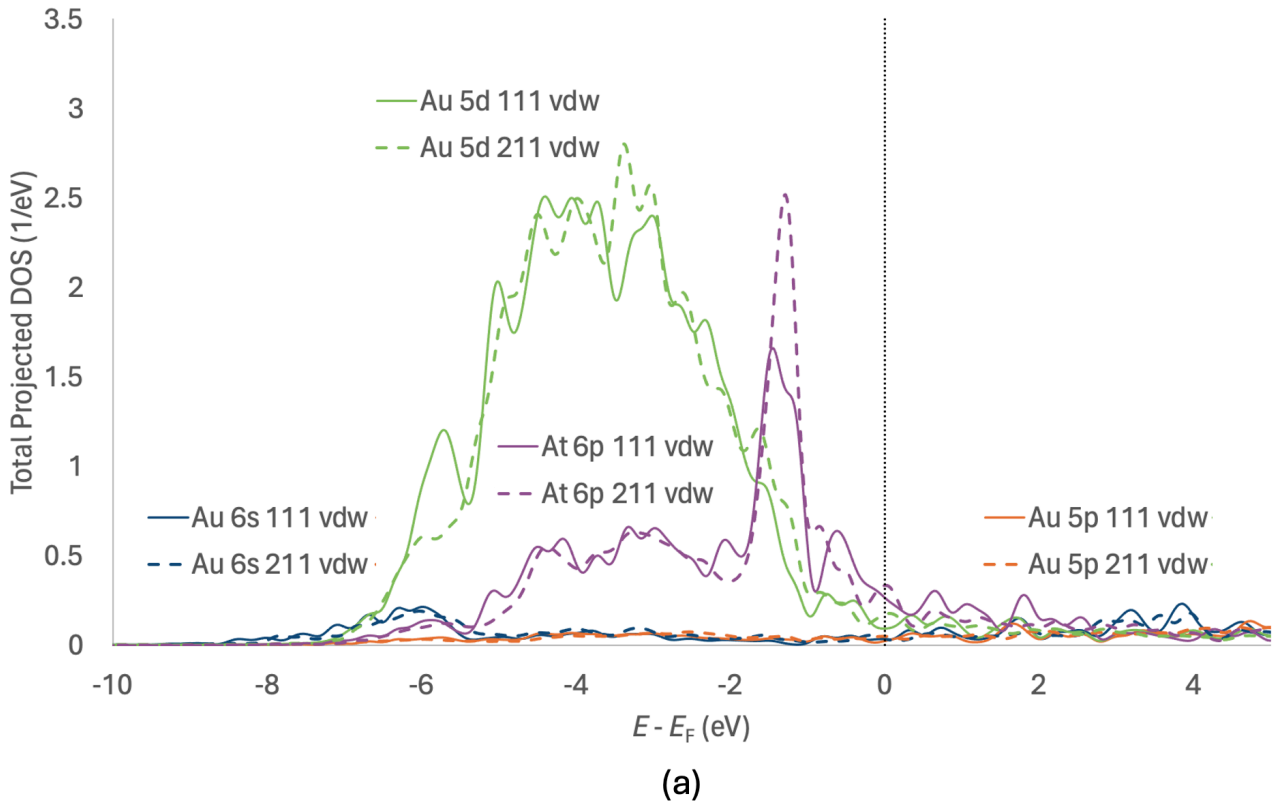

(a)

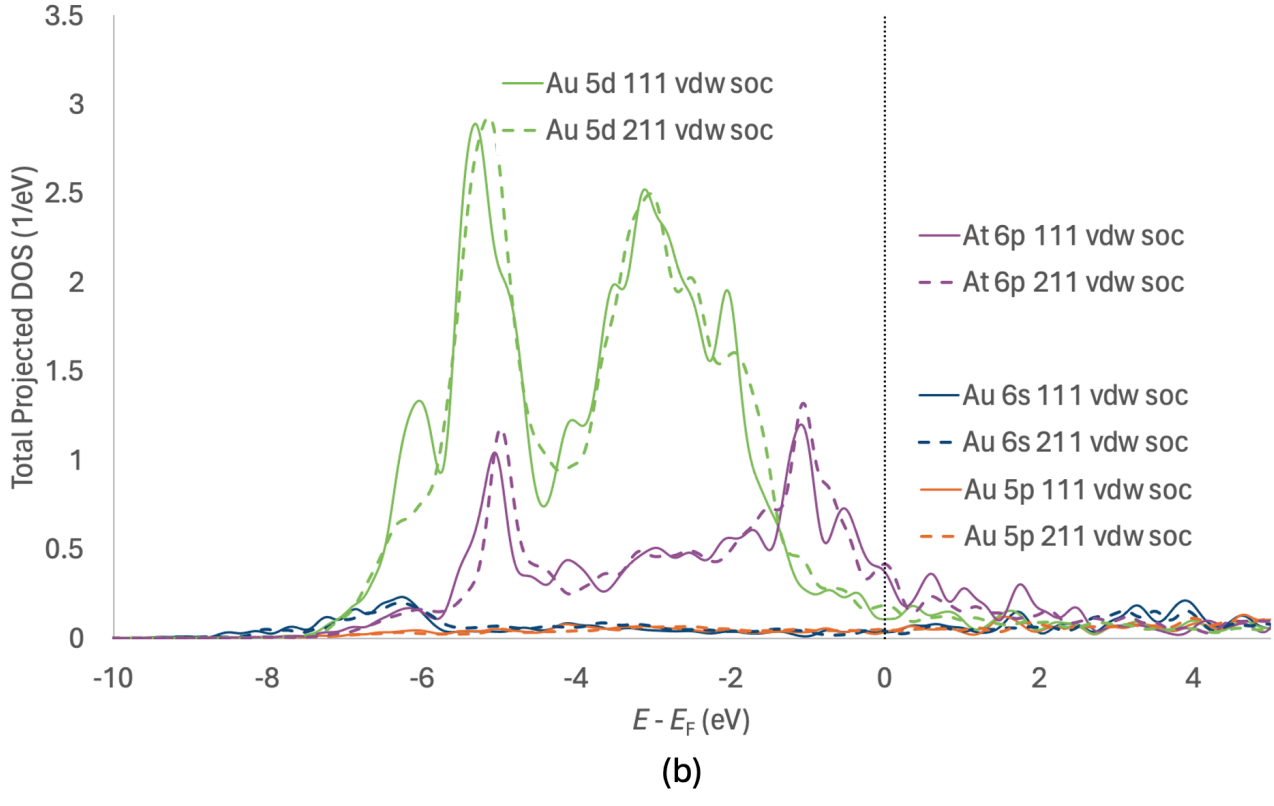

(b)

Figure 4-6. Comparison of densities of states for At/Au(211) and At/Au(111). (a) with vdW and (b) with vdW and SOC.

4.3 Conclusion for chapter 4

I presented the results that Au(211) can adsorb both astatine and iodine more strongly and stably than Au(111). This is due to the Au(211) surface being more reactive than the Au(111) surface based on calculations of the work function. Both astatine and iodine adsorbs covalently on Au(211) with hybridization of the iodine's 5p and astatine's 6p orbitals with the gold 5d in the energy range of -4.5 eV to -2 eV and gold 6s around the energy range of -6 eV. Consideration of SOC shows a more fitting hybridization but ultimately does not affect the adsorption energy strength calculated previously. Diffusion calculations also show that adsorption on Au(211) is more stable than Au(111) in that the adsorbate is less likely to diffuse after adsorption on the edge-bridge site of Au(211). Therefore, based on this study, nanoparticles which have more edges and sharp interfaces can adsorb astatine more strongly and keep them stable.

The findings from this simulation can be used to determine the optimal shape and structure of the gold nanoparticles used for TAT applications. Current state of experimental finding is based only on the size of the AuNPs, which, while useful, is not comprehensive in understanding the best adsorption criteria for astatine on gold. Since we can employ theoretical calculations to look into the details of such reaction, it becomes an important endeavor to study various combinations in order to help experimentalists realize these findings in actual conditions.

References

[1] J. Tanudji, S. M. Aspera, H. Kasai, M. Okada, T. Ogawa, and H. Nakanishi, e-J. Surf. Sci. Nanotechnol. 22 (2024) 38-45.

[2] A. M. Rodriguez, G. Bozzolo, and J. Ferrante, Surf. Sci. 289 (1993) 100-126.

[3] J. Tanudji, S. M. Aspera, and H. Kasai, e-J. Surf. Sci. Nanotech. 21 (2023) 318-323.

Chapter 5

Conclusion

5.1 Summary of findings

This dissertation has studied the adsorption of astatine on gold surfaces and its comparison with iodine on the same gold surfaces. Astatine was found to adsorb quite stably on gold due to the covalent bonding between astatine and gold. Since astatine is a halogen, another similar radionuclide, iodine, is used for comparison. Both elements are found to exhibit similar properties but also, due to the heavy nature of astatine, its electronic character is slightly different than iodine.

In chapter 2, I showed that astatine is able to adsorb on flat Au(111). The adsorption is covalent, with the 6p orbital of astatine hybridizing with the gold 5d in the energy range of -4.5 eV to -2 eV, as well as with the gold 6s in the energy range of -6 eV. Bader charge calculation indicate that astatine is loses a small amount of charge after adsorption, classifying it as a charge donor, although only very slightly. Due to the heavy nature of astatine, spin-orbit coupling (SOC) correction is considered in the calculation, but the change that it brings to the adsorption energy is small enough to be negligible. Calculations involving van der Waals (vdW) correction is found to yield more accurate energies, comparable to experimental results. The effect of SOC is manifest in the electronic states, where the splitting of the gold 5d and astatine 6p, otherwise unobserved if doing a scalar-relativistic calculation, produces a more fitting hybridization between the two orbitals mentioned earlier.

In chapter 3, a comparison of the previous system is made by replacing astatine with iodine. The aim is to provide an idea as to the effect of a lighter radionuclide adsorbing on gold. Iodine, having no electrons in 4f orbital, contrasts with astatine with a fully occupied 4f orbital. The result found that iodine adsorbs less strongly than astatine, which is unexpected since earlier studies show a decreasing adsorption energy as we go down the periodic table. This may be due to the lanthanide contraction found in astatine, which is able to keep the atomic size from getting larger. Electrons occupying the 4f orbital are also less effective at screening the core charges, making the valence shells more compact.

In chapter 4, I conducted a study on the effect of different surface facets in order to find a more optimum surface for adsorption. The Au(211) is chosen since it has a short terrace of Au(111), with a step that allows for a break in the flat surface. The result is that both astatine and iodine can adsorb more strongly on the stepped edges than on flat surface. This is due to the Au(211) being more reactive than the Au(111), as shown by the slightly weaker work function. The stabilities of the adsorption on these surfaces are also calculated, with adsorption on Au(211) being much more stable. The energy barrier that an adsorbate needs to overcome is higher in the Au(211) than in Au(111), effectively making the adsorbate stay in that position and not moving about easily.

Based on the above findings, I found that gold can be a good carrier for astatine in TAT applications. The inherent inertness of gold means the gold is unlikely to interact with other compounds and therefore is deemed to be biocompatible. In addition, the bonding strength afforded by gold towards astatine is strong enough to hold astatine until they reach the targeted areas. As

used in experiments, gold can be made into nanoparticles, which can be deployed inside the patients' bodies to perform treatments. In this study, the gold nanoparticles have been modeled as surfaces. This was based on findings that for nanoparticles of sizes above c.a. 2.7 Å, the adsorption energy obtained for a nanoparticle was found to correspond with a surface equivalent. Therefore since the experimental results were obtained using nanoparticles of at least 5 Å diameter, the results from the modeling is valid.

Finally, auxiliary compounds such as drugs, tracking particles, etc. can be attached to gold alongside astatine. With the additional advantages that gold has, e.g., surface plasmon resonance, producing reactive oxygen species to aid in destroying cancer cells, and others, the use of gold is one important aspect in this methodology. No doubt more insights will be made and applied in the future, as more of these aspects are studied.

5.2 Future works

The current state of experimental TAT is quite complex, with many different groups studying different aspects of the treatment itself. Among the aspects are the different use of targeting compounds and clinical trials involving only astatine without gold nanoparticles. There are also ideas about harnessing other materials to be carriers. With such diverse interest, researches in TAT are bound to generate much more new information as well as best practices that allow it to be a viable methodology in cancer therapy.

Since this study only looks at a limited aspect, there are many potential researches that can be undertaken. The decay process has been neglected to focus attention to the adsorption phenomenon. Simplification is also employed in the form of surfaces; as gold nanoparticle sizes become smaller, finite-sized effects cannot be ignored and a full simulation using three-dimensional model is required. The addition of engineered defects may also provide an interesting result since from the study, we know that a pristine surface has less room for the surface atoms to maneuver. Additionally, there is a lack of experimental results for different variables since many of the experiments are performed by biologists who are more interested in astatine's efficacy than the underlying physical fundamentals.

Moving out of the theoretical sphere, there are many issues to be tackled in its application. From astatine production capabilities to potential patient antibodies disrupting its application, it takes many people of different background and specialities to study this methodology. A review has been written to provide an overview of the current state of development as well as problems that come up before astatine's application can be approved for regular use in treating cancers [Chapter. 1 ref. 21]. Future developments for this initiative should therefore be undertaken to advance both fields of study.

Appendices

Appendix A - Theoretical foundation of density functional theory

A.1 Born-Oppenheimer approximation of a time-independent Schrödinger equation

All systems by nature contain energies, and those energies can be conveyed using the Schrödinger equation of the form

$$\hat{H}\Psi\left\{\vec{R_i}, \vec{r_i}\right\} = E\Psi\left\{\vec{R_i}, \vec{r_i}\right\} \tag{A1}$$

where Ψ is the many-body wavefunction based on the coordinates of the particles, $\vec{R_i}$ is the coordinate of the i^{th} nucleus, $\vec{r_i}$ is the coordinate of the i^{th} electron, and E is the energy eigenvalue. $\hat{H}$ is the Hamiltonian operator which can be further divided into

$$\hat{H} = \hat{T}_{elec} + \hat{T}_{nuc} + \hat{V}_{elec-nuc} + \hat{V}_{nuc-nuc} + \hat{V}_{elec-elec} \tag{A2}$$

where $\hat{T}_{elec}$ is the electronic kinetic energy operator, $\hat{T}_{nuc}$ is the nuclear kinetic energy operator, $\hat{V}_{elec-nuc}$ is the electron-nuclear potential energy operator, $\hat{V}_{nuc-nuc}$ is the nuclear-nuclear potential energy operator, and $\hat{V}_{elec-elec}$ is the electron-electron potential energy operator. Fully writing the terms, equation (A2) becomes

$$\hat{H} = -\frac{\hbar^2}{2m}\sum_{i=1}^{N}\nabla_i^2 - \frac{\hbar^2}{2}\sum_{I=1}^{M}\frac{1}{M_I}\nabla_I^2 - \frac{1}{4\pi\epsilon_0}\sum_{i-1}^{N}\sum_{I=1}^{M}\frac{Z_I e^2}{r_{iI}} + \frac{1}{2}\frac{1}{4\pi\epsilon_0}\sum_{i\neq j}^{N}\frac{e^2}{r_{ij}} - \frac{1}{2}\frac{1}{4\pi\epsilon_0}\sum_{I\neq J}^{M}\frac{Z_I Z_J e^2}{r_{IJ}} \tag{A3}$$

where $\hbar$ is the reduced Planck constant, m is the mass of the electron, M_I is the mass of the I^{th} nucleus, i and j are counters for electrons that have a maximum value of N, I and J are counters for nuclei that have a maximum value of M, $\frac{1}{4\pi\epsilon_0}$ is a constant found in Coulomb's law, Z is a multiplier for the charges found in the nucleus, and r_i and R_I give the distances from the origin point of the i^{th} electron and I^{th} nucleus respectively.

Due to the large ratio of mass between the nuclei and the electrons, we can approximate the motion of the particles by assuming the nuclei to be fixed while the electrons are moving in the constant external potential $V(r)$. This approximation makes $\hat{T}_{nuc} \approx 0$ and $\hat{V}_{nuc-nuc} = \frac{1}{4\pi\epsilon_0}\sum_{I<J}\frac{Z_I Z_J}{R_{IJ}}$, which then simplifies equation (A3) as

$$\hat{H}_{elec} = \hat{T}_{elec} + \hat{V}_{elec-nuc} + \hat{V}_{elec-elec} \tag{A4a}$$

$$\hat{H}_{elec} = -\frac{\hbar^2}{2m} + \frac{1}{4\pi\epsilon_0}\sum_{i=1}^{N}\sum_{I=1}^{M}\frac{Z_I e}{r_{iI}} + \frac{1}{2}\frac{1}{4\pi\epsilon_0}\sum_{i\neq j}^{N}\frac{e^2}{r_{ij}} \tag{A4b}$$

A.2 Hohenberg-Kohn theorems

Before going deeper, we have to establish a new parameter called the electron density. The electron density is defined as

$$\int \rho(\vec{r})d\vec{r} \equiv N \tag{A5}$$

where $\rho(\vec{r})$ is the electron density and the integral over the volume of the system yield N, the total number of electrons. The Hohenberg-Kohn theorems state that

1. An external potential $V_{ext}(\vec{r})$ can only correspond to one particular $\rho(\vec{r})$.
2. Given a particular system, there exists a ground state electron density, $\rho(\vec{r})$, which minimizes the energy.

The proof for number 1:
Consider two different external potentials $\hat{V}_{ext}$ and $\hat{V}'_{ext}$. These potentials correspond to two different Hamiltonians $\hat{H}$ and $\hat{H}'$ respectively, whose ground state electron densities are the same even though the normalized wave functions Ψ and Ψ' are different. This yields

$$E_0 = \left\langle \Psi \middle| \hat{H} \middle| \Psi \right\rangle < \left\langle \Psi' \middle| \hat{H} \middle| \Psi' \right\rangle = \left\langle \Psi' \middle| \hat{H} + \hat{V} - \hat{V}' \middle| \Psi' \right\rangle$$

$$E_0 < \left\langle \Psi' \middle| \hat{H}' \middle| \Psi' \right\rangle + \int \rho(\vec{r}) \left[v(\vec{r}) - v'(\vec{r}) \right] d\vec{r}$$

$$E_0 < E'_0 + \int \rho(\vec{r}) \left[v(\vec{r}) - v'(\vec{r}) \right] d\vec{r} \tag{A6a}$$

The reverse:

$$E'_0 = \left\langle \Psi' \middle| \hat{H}' \middle| \Psi' \right\rangle < \left\langle \Psi \middle| \hat{H}' \middle| \Psi \right\rangle = \left\langle \Psi \middle| \hat{H} + \hat{V}' - \hat{V} \middle| \Psi \right\rangle$$

$$E'_0 < E_0 + \int \rho(\vec{r}) \left[v'(\vec{r}) - v(\vec{r}) \right] d\vec{r}$$

$$E'_0 < E_0 - \int \rho(\vec{r}) \left[v(\vec{r}) - v'(\vec{r}) \right] d\vec{r} \tag{A6b}$$

Combining equations (A6a) and (A6b) gives

$$E_0 + E'_0 < E'_0 + E_0 \tag{A7}$$

which does not make sense. Ergo, there is a one-to-one mapping between external potential $V_{ext}(\vec{r})$ and electron density $\rho(\vec{r})$.

The ground state energy can be written as

$$E\left[\rho\right] = E_{elec-enuc}\left[\rho\right] + F\left[\rho\right] \tag{A8}$$

where $F\left[\rho\right] = T\left[\rho\right] + E_{elec-elec}\left[\rho\right]$. $E_{elec-elec}$ can be decomposed into the classical and non-classical parts:

$$E_{classical}\left[\rho\right] = \frac{1}{2}\frac{e^2}{4\pi\epsilon_0}\iint \frac{\rho(\vec{r}_1)\rho(\vec{r}_2)}{r_{12}} d\vec{r}_1 d\vec{r}_2 \tag{A9}$$

where the classical part is just the Coulomb interaction.

The proof for number 2:
For a trial density $\tilde{\rho}$, $E_0 \leq E\left[\tilde{\rho}\right]$

$$E_0 \equiv E\left[\rho\right] \leq \left\langle \tilde{\Psi} \middle| \hat{H} \middle| \tilde{\Psi} \right\rangle = F\left[\tilde{\rho}\right] + \int \tilde{\rho} V_{elec-nuc}(\vec{r}) d\vec{r} = E\left[\tilde{\rho}\right] \tag{A10}$$

where $F\left[\tilde{\rho}\right] = \left\langle \tilde{\Psi} \middle| \hat{F} \middle| \tilde{\Psi} \right\rangle = \left\langle \tilde{\Psi} \middle| T\left[\tilde{\rho}\right] + E_{elec-elec}\left[\tilde{\rho}\right] \middle| \tilde{\Psi} \right\rangle$

Therefore, we can separate equation (A10) into

$$E\left[\rho\right] = \int \rho(\vec{r}) v_{elec-elec} \vec{r} d\vec{r} + \left\langle \Psi \middle| T\left[\rho\right] + E_{elec-elec}\left[\rho\right] \middle| \Psi \right\rangle \tag{A11a}$$

$$E\left[\tilde{\rho}\right] = \int \tilde{\rho}(\vec{r}) v_{elec-elec} \vec{r} d\vec{r} + \left\langle \tilde{\Psi} \left| T\left[\tilde{\rho}\right] + E_{elec-elec}\left[\tilde{\rho}\right] \right| \tilde{\Psi} \right\rangle \quad \text{(A11b)}$$

and when $\tilde{\rho} = \rho$, then equation (A11a) is equal to (A11b), and the system's ground energy is obtained.

A.3 Kohn-Sham equations

From equation (A8) and (A9)

$$E\left[\rho\right] = T\left[\rho\right] + \frac{1}{2}\frac{e^2}{4\pi\epsilon_0}\int\int \frac{\rho(\vec{r}_1)\rho(\vec{r}_2)}{r_{12}} d\vec{r}_1 d\vec{r}_2 + E_{non-classical}\left[\rho\right] + \int \rho(\vec{r}) V_{elec-nuc}(\vec{r}) d\vec{r} \quad \text{(A12)}$$

Kohn and Sham now introduces a non-interacting single particle reference system with

$$\rho_s = \sum_{i=1}^{N} \left|\Phi_i(\vec{r})\right|^2 = \sum_{i=1}^{N} \Phi_i^*(\vec{r})\Phi_i(\vec{r}) = \rho(\vec{r}) \quad \text{(A13)}$$

$$\text{and } T_s\left[\rho\right] = -\frac{\hbar^2}{2m}\sum_{i=1}^{N}\left\langle \Phi_i \left| \nabla^2 \right| \Phi_i \right\rangle \quad \text{(A14)}$$

where Φ_is are the orbitals of the non-interacting electrons. Based on equation (A3), a Langrange multiplier, μ, is chosen such that

$$\frac{\delta}{\delta\rho(\vec{r})}\left\{ E\left[\rho(\vec{r})\right] - \mu\int\rho(\vec{r})d\vec{r} \right\} = 0$$

$$\Rightarrow \frac{\delta}{\delta\rho(\vec{r})} E\left[\rho(\vec{r})\right] = \mu \quad \text{(A15)}$$

$T\left[\rho\right]$ and $T_s\left[\rho\right]$ is different due to the latter assuming a non-interaction between electrons. So,

$$F\left[\rho\right] = T\left[\rho\right] + E_{elec-elec}\left[\rho\right] = T\left[\rho\right] + E_{classical}\left[\rho\right] + E_{non-classical}\left[\rho\right] \quad \text{(A16)}$$

With some manipulation, we get

$$F\left[\rho\right] = T_s\left[\rho\right] + E_{classical}\left[\rho\right] + E_{XC} \quad \text{(A17)}$$

where we define the exchange-correlation energy, E_{XC}, as $T\left[\rho\right] - T_s\left[\rho\right] + E_{non-classical}\left[\rho\right]$. Combining equations (A8) and (A17),

$$E\left[\rho(\vec{r})\right] = T_s\left[\rho(\vec{r})\right] + \frac{1}{2}\frac{e^2}{4\pi\epsilon_0}\int\int\frac{\rho(\vec{r}_1)\rho(\vec{r}_2)}{r_{12}} d\vec{r}_1 d\vec{r}_2 + E_{XC}\left[\rho\right] + \int\rho(\vec{r}) V_{elec-nuc}(\vec{r}) d\vec{r} \quad \text{(A18)}$$

Substituting $\vec{r}$ for $\vec{r}_1$, $\vec{r}'$ for $\vec{r}_2$, into equation (A18), and the result into equation (A15) gives

$$\frac{\delta}{\delta\rho(\vec{r})} T_s\left[\rho(\vec{r})\right] + V_{eff}(\vec{r}) = \mu \quad \text{(A19)}$$

$$\text{where } V_{eff}(\vec{r}) = V_{elec-nuc}(\vec{r}) + \frac{e^2}{4\pi\epsilon_0}\int\frac{\rho(\vec{r}')}{\left|\vec{r} - \vec{r}'\right|} d\vec{r}' + V_{XC}(\vec{r}) \quad \text{(A20)}$$

$$\text{of which } V_{XC}(\vec{r}) = \frac{\delta E_{XC}[\rho(\vec{r})]}{\delta\rho} \quad \text{(A21)}$$

The Kohn-Sham equation is

$$\left(-\frac{\hbar^2}{2m}\nabla^2 + V_{eff}(\vec{r})\right)\Phi_i = \varepsilon_i\Phi_i(\vec{r}) \tag{A22}$$

where $E_0 = \sum_{i=1}^{N} \varepsilon_i$,

$V_{eff}(\vec{r}) = V_{elec-nuc}(\vec{r}) + \frac{e^2}{4\pi\epsilon_0}\int \frac{\rho(\vec{r}')}{\left|\vec{r} - \vec{r}'\right|} d\vec{r}' + V_{XC}(\vec{r})$, and

$\rho_s = \sum_{i=1}^{N} \left|\Phi_i(\vec{r})\right|^2$.

A.4 Exchange-correlation functional

The exchange-correlation functional embodies all the unknown terms due to the assumptions introduced by the Kohn-Sham equations. Due to the complexities obtaining an exact formulation, an ansatz for this functional must be utilized and iteratively solved in order to get a convergence on the energies of both sides. This procedure is known as a "self-consistent field cycle."

The simplest approximation is made from using the homogenous electron gas as the basis. This is known as the local density approximation (LDA) and is in the form of

$$E_{XC}^{LDA}[\rho] = \int \rho(\vec{r})\varepsilon_{XC}\left(\rho(\vec{r})\right) d\vec{r} \tag{A23}$$

where $\varepsilon_{XC}\left(\rho(\vec{r})\right)$ is the exchange-correlation energy per particle of a homogenous electron gas of density $\rho(\vec{r})$ and can be decomposed as

$$\varepsilon_{XC}\left(\rho(\vec{r})\right) = \varepsilon_X\left(\rho(\vec{r})\right) + \varepsilon_C\left(\rho(\vec{r})\right) \tag{A24}$$

The exchange term for the homogenous electron gas can be obtained analytically, and the correlation term can be obtained from quantum Monte Carlo simulations.

Since any real systems are not homogenous, i.e. having spatially varying $\rho(\vec{r})$, the addition of a correction to this approximation should yield results more representative of the system. This correction comes in the form of the electron density, $\rho(\vec{r})$, and its gradient, $\nabla\rho(\vec{r})$, and is called the generalized gradient approximation (GGA) with the form

$$E_{XC}^{GGA}[\rho] = \int \varepsilon_{XC}\left(\rho(\vec{r}), \nabla\rho(\vec{r})\right) d\vec{r} \tag{A25}$$

There are many types of GGA exchange-correlation functionals that have been developed. Using GGA, consistent results for molecular geometry and energies can be obtained.

A.5 Spin orbit coupling

Spin orbit coupling (SOC) is the interaction between the spin of the electron and the orbital angular momentum of the electron. Consideration of this phenomenon causes the splitting of energy levels of the electron and the disappearance of conventional spin directions. While this can be obtained from solving the Dirac equation for relativistic quantum mechanics, an easier method using

approximations can be employed to give a relatively accurate result. The following is a simplified derivation based on an electron bound to a hydrogen-like atom.

The energy of a magnetic moment in a magnetic field is given by

$$\hat{H} = -\vec{\mu}\cdot\vec{B} \tag{A26}$$

where $\vec{B}$ is the magnetic field, $\vec{\mu}$ is the magnetic dipole moment and can be expressed as $\vec{\mu} = \gamma\vec{S}$, in which γ is the gyromagnetic ratio and $\vec{S}$ is the spin angular momentum. When a magnetic dipole is placed in a magnetic field $\vec{B}$, it experiences a torque $\vec{\mu} \times \vec{B}$ which tends to line it up parallel to the field. Equation (A26) then becomes

$$\hat{H} = -\gamma\vec{S}\cdot\vec{B} \tag{A27}$$

The magnetic field of a proton can be obtained via the Biot-Savart law as $B = \frac{\mu_0 I}{2r}$ with an effective current $I = \frac{e}{T}$, e being the charge of the proton and T the period of the orbit. On the other hand, the orbital angular momentum of the electron (in the rest frame of the nucleus) is $L = rmv = 2\pi m\frac{r^2}{T}$. Moreover, from this frame of reference, the nucleus (i.e. proton) is revolving around the electron, which induces a magnetic field in the same direction as the orbital angular momentum (figure A1 left side).

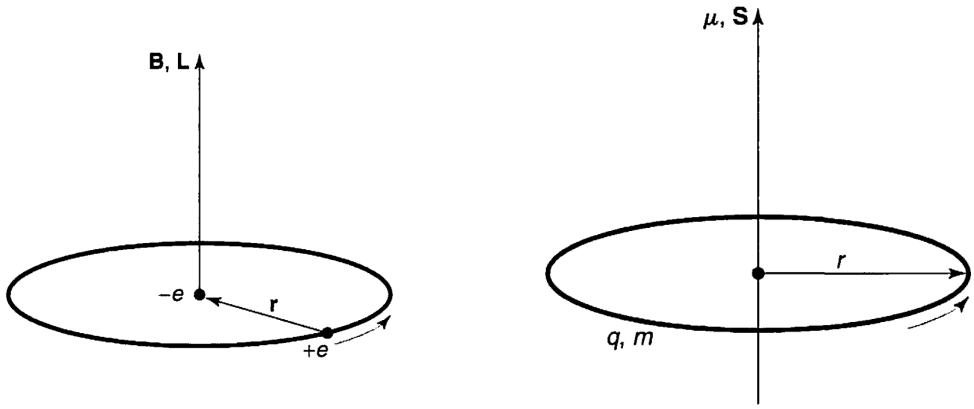

Figure A1. (Left) Hydrogen-like atom, from the electron's perspective. (Right) A ring of charge, rotating about its axis. [1]

The magnetic field can then be expressed as

$$\vec{B} = \frac{1}{4\pi\epsilon_0}\frac{e}{mc^2r^3}\vec{L} \tag{A28}$$

For the magnetic dipole of the electron, consider a charge q smeared out around a ring of radius r, which rotates about the axis with period T (figure A1 right side). The magnetic dipole moment of the ring is

$$\mu = \frac{q}{T}\pi r^2 \tag{A29}$$

The angular momentum is the moment of inertia times the angular velocity:

$$S = \frac{2\pi}{T}mr^2 \tag{A30}$$

The gyromagnetic ratio for this configuration is then

$$\frac{\mu}{S} = \frac{q}{2m} \tag{A31}$$

If the directions of q and S are the same (i.e. the same charge) then $\mu_+ = \frac{q}{2m}S$; if not, it is $\mu_- = -\frac{q}{2m}S$.

But it is found that $\vec{\mu_e} = -\frac{e}{m}\vec{S}$; this extra factor of 2 can be explained by solving Dirac's relativistic equation. However, we are going to use an appropriate kinematic correction, known as Thomas precession to get the answer as

$$H'_{SO} = \left(\frac{e^2}{8\pi\epsilon_0}\right)\frac{1}{m^2c^2r^3}\vec{S}\cdot\vec{L} \tag{A32}$$

However, this spin-orbit interaction is based completely on classical physics and thus the commutation between $\vec{L}$ and $\vec{S}$ will change the result. The total angular momentum $\vec{J} = \vec{L} + \vec{S}$. The eigenstates of L_Z and S_Z are not good states to use in perturbation theory, but the eigenstates of L^2, S^2, J^2, and J_Z are.

$$J^2 = \left(\vec{L} + \vec{S}\right)\cdot\left(\vec{L} + \vec{S}\right) = L^2 + S^2 + 2\vec{L}\cdot\vec{S}$$

$$\vec{L}\cdot\vec{S} = \frac{1}{2}\left(J^2 - L^2 - S^2\right) \tag{A33}$$

Therefore the eigenvalues of $\vec{L}\cdot\vec{S}$ are

$$\frac{\hbar}{2}\left[j(j+1) - l(l+1) - s(s+1)\right] \tag{A34}$$

for which $s = \frac{1}{2}$. Meanwhile $\left\langle\frac{1}{r^3}\right\rangle = \frac{1}{l\left(l+\frac{1}{2}\right)(l+1)n^3a^3}$, and we get

$$E'_{SO} = \left\langle H'_{SO}\right\rangle = \frac{e^2}{8\pi\epsilon_0}\frac{1}{m^2c^2}\frac{\frac{\hbar}{2}\left[j(j+1) - l(l+1) - \frac{3}{4}\right]}{l\left(l+\frac{1}{2}\right)(l+1)n^3a^3} \tag{A35}$$

Reference for appendix A

[1] D. J. Griffiths, Introduction to Quantum Mechanics, 2nd Ed., Pearson Education (2005)

Appendix B - Calculation details

Theoretical calculations were conducted using DFT as implemented in the DFT software Vienna Ab-initio Software Package (VASP) [1,2]. The electronic one-particle wave-function was expanded to an energy cutoff of 400 eV. A convergence threshold for the self-consistent field calculation was set to 10^{-5} eV, meaning that the calculation was considered converged if the energy difference between the steps was less than 10^{-5} eV. I used pseudopotentials with Perdew-Burke-Ernzerhof generalized gradient approximation exchange correlation functional and the projected augmented wave method to describe the modeling of the core electrons [3,4].

For the partial filling of the electronic orbitals, I used the method of Methfessel-Paxton order 1 with a smearing width of 0.2 eV. The integration for the first Brillouin zone was performed by a mesh of $5 \times 5 \times 1$ *k*-points with a Monkhorst-pack sampling scheme [5]. Calculations involving van der Waals interaction employed the DFT-D3 code developed by Grimme *et al* [6]. Calculations involving spin orbit coupling (SOC) were done from the VASP input file, which automatically adjusts the pseudopotential to be fully relativistic [7].

The relaxation of the top half of the slabs were done using the residual minimization method - direct inversion in the iterative subspace algorithm [8,9]. I also included the electronic dipole correction along the c-axis to take into account possible effects of charge interactions between the repeated Au slab layers.

Lattice constant for gold slab was found to be 4.16 Å for non-vdW calculation, 4.12 Å for vdW calcultion, and 4.10 Å for vdW + SOC calculation, all of which are consistent with the values in the CRC Handbook of Chemistry and Physics [10].

Finally, Bader charge calculations are performed before and after adsorption to obtain the charge transfers for each atom [11]. The fine fast Fourier transform grid mesh for these calculations was increased to obtain a resolution of 0.01 charges in the final results, which is more accurate than the default setting. The simulation considers Au to have 11 valence electrons in the electronic configuration $5d^{10}6s^{1}$, iodine to have 7 valence electrons in the $5s^{2}5p^{5}$ configuration, and astatine to also have 7 valence electrons in the $6s^{2}6p^{5}$ configuration.

Reference for appendix B

[1] G. Kresse and J. Furthmüller, Phys. Rev. B 54 (1996) 11169-11186.
[2] G. Kresse and J. Furthmüller, Comput. Mater. Sci. 6 (1996) 15-50.
[3] J. Perdew, K. Burke, and M. Ernzerhof, Phys. Rev. Lett. 77 (1996) 3865-3868.
[4] P. E. Blöchl, Phys. Rev. B 50 (1994) 17953-17979.
[5] H. J. Monkhrst and J. D. Pack, Phys. Rev. B 13 (1976) 5188-5192.
[6] S. Grimme, S. Ehrlich, and L. Goerigk, J. Comput. Chem. 32 (2011) 1456-1465.
[7] D. Hobbs, G. Kresse, and J. Hafner, Phys. Rev. B 62 (2000) 11556-11570.
[8] D. M. Wood and A. Zunger, Phys Rev. A 18 (1985)1343-1359.
[9] P. Pulay, Chem. Phys. Lett. 73 (1980) 393-398.
[10] D. R. Lide (Ed.), CRC Handbook of Chemistry and Physics, 86th ed. (Taylor and Francis Group, Florida, 2005) pp. 4-150.
[11] G. Henkelman, A. Arnaldson, and H. Jónsson, Comput. Mater. Sci. 36 (2006) 354.

List of publications

1. T. Kasai, B. Muthiah, X-H. Po, C-C. Yan, K-C. Lin, J. Tanudji, and W. A. Diño, Pattern analysis of the impact-parameter dependent trajectories for the H + H2 exchange reaction at T = 3 and 300 K: A characteristic propensity for reactive versus nonreactive trajectories found in the time-dependent interaction potential and a roaming-like libration motion at cold temperature. J. Chinese Chem. Soc. 69 (2022) 630-645.

2. J. Tanudji, S. M. Aspera, H. Kasai, M. Okada, T. Ogawa, and H. Nakanishi, Computational Nanomaterials Design: Towards the Realization of Nanoparticle use in Radiotherapy – Case Study 2: Adsorption states of At on Au(111) Surface. Phys. Sci. Int. J. 26 (2022) 1-10.

3. J. Tanudji, S. M. Aspera, and H. Kasai, Theoretical comparison study of iodine and astatine adsorption on Au(111) surface. e-J. Surf. Sci. Nanotech. 21 (2023) 318-323.

4. J. Tanudji, S. M. Aspera, H. Kasai, M. Okada, T. Ogawa, and H. Nakanishi, Surface facet effect on the adsorption of iodine and astatine on gold surface. e-J. Surf. Sci. Nanotech. 22 (2023) 38-45.

5. J. Tanudji, H. Kasai, M. Okada, T. Ogawa, S. M. Aspera, H. Nakanishi, 211At on Gold Nanoparticles for Targeting Radionuclide Therapy Application, Phys. Chem. Chem. Phys. 26 (2024) 12915-12927.

List of conferences attended

1. Jeffrey Tanudji, Hideaki Kasai, Novianto Nur Hidayat, and Hiroshi Nakanishi, “Comparison of quantum mechanical tunneling of Hydrogen through a single graphene sheet and Palladium thin film”, the Physical Society of Japan Annual (76th) Spring 2021 Meeting, Online (2021-03-13)

2. Jeffrey Tanudji and Hideaki Kasai, “A Theoretical Comparison of Potential Energy for Hydrogen Diffusion Through Three-layered Pd(111) and Five-layered Pd(111)”, the Physical Society of Japan Annual (76th) Fall 2021 Meeting, Online (2021-09-23)

3. Jeffrey Tanudji, Hideaki Kasai, Michio Okada, Tetsuo Ogawa, Susan Meñez Aspera, and Hiroshi Nakanishi, “Adsorption State of Iodine on Gold (111) Surface”, the Physical Society of Japan Annual (77th) Spring 2022 Meeting, Online (2022-03-15)

4. Jeffrey Tanudji, Hideaki Kasai, Michio Okada, Tetsuo Ogawa, Susan Meñez Aspera, and Hiroshi Nakanishi, “Adsorption State of Iodine on Gold (111) Surface”, the 69th JSAP Spring Meeting 2022, Online (2022-03-22)

5. Jeffrey Tanudji, Hideaki Kasai, Michio Okada, Tetsuo Ogawa, Susan Meñez Aspera, and Hiroshi Nakanishi, “Adsorption of Iodine on Au(111) surface: coverage effect”, the 22nd International Vacuum Congress IVC-22 Conference, Sapporo, Hokkaido, Japan (2022-09-14) (Poster presentation)

6. Jeffrey Tanudji, Hideaki Kasai, Michio Okada, Tetsuo Ogawa, Susan Meñez Aspera, and Hiroshi Nakanishi, “Comparison of Astatine and Iodine adsorption on Au(111) surface”, the 22nd International Vacuum Congress IVC-22 Conference, Sapporo, Hokkaido, Japan (2022-09-14)

7. Jeffrey Tanudji, Hideaki Kasai, Michio Okada, Tetsuo Ogawa, Susan Meñez Aspera, and Hiroshi Nakanishi, “Comparison of Astatine and Iodine adsorption on Au(111) surface”, the 83rd JSAP Autumn Meeting 2022, Online (2022-09-21)

8. Jeffrey Tanudji and Hideaki Kasai, “Effect of Surface Facet on Iodine and Astatine Adsorption on Gold Nanoparticle”, the 70th JSAP Spring Meeting 2023, Online (2023-03-15)

9. Jeffrey Tanudji, Susan Meñez Aspera, Hideaki Kasai, Michio Okada, Tetsuo Ogawa, and Hiroshi Nakanishi, “Adsorption State of Iodine and Astatine on Gold Surface”, Short-lived radionuclide symposium (短寿命RI利用研究シンポジウム), Suita, Osaka, Japan (2023-08-02) (Poster presentation)

10. Jeffrey Tanudji and Hideaki Kasai, “Effect of Surface Facet on Iodine and Astatine Adsorption on Gold Nanoparticle II”, the 84th JSAP Autumn Meeting 2023, Online (2023-09-21)

11. Jeffrey Tanudji, Susan Aspera, Hideaki Kasai, Michio Okada, Tetsuo Ogawa, and Hiroshi Nakanishi, “Coverage effect of iodine and astatine adsorption on Au surfaces”, the 84th JSAP Autumn Meeting 2023, Online (2023-09-21)

12. 笠井 秀明, タヌジ ジェフリ, 岡田 美智雄, 小川 哲夫, スーサン アスペラ, 中西 寛, “Effects of “Lanthanide Shrinkage” on Surface Adsorption of Astatine on Gold and Platinum”, the Physical Society of Japan 2024 Spring Meeting, Online (2024-03-20)

13. Jeffrey Tanudji, 笠井 秀明, 岡田 美智雄, 中西 寛, “Effect of d-orbitals on the adsorption of astatine on biocompatible metals” the 71st JSAP Spring Meeting 2024, Online (2024-03-25)

Acknowledgments

The road to this thesis is long and would not have been possible without the assistance of many people. This short section is dedicated to them and their memories.

This thesis is particularly dedicated to the memory of my late father, who passed away from the disease that his son is currently researching on. While it may be too late for him, it is my sincere wish that this work can be beneficial for future generations and more people can be saved from this disease.

First I would like to thank Prof. Wilson A. Diño as my supervisor and the many discussions we had. I would also like to thank Prof. Hideaki Kasai for suggesting this topic to me and supporting me in this research. The time and effort he afforded to me allowed me to finish this thesis in its entirety.

Next, I would like to thank Profs. Yuji Kuwahara, Nobuya Mori, and Michio Okada as my panelists. I am grateful for their willingness to take time off their busy schedules and provide many invaluable comments on my thesis. I wish to thank Prof. Hiroshi Nakanishi for his generosity in allowing me to perform the calculations in his Nano lab at National Institute of Technology, Akashi College. Further calculations were performed in the Yukawa Institute of Theoretical Physics in Kyoto University.

I would like to express my gratitude to Prof. Kazuyuki Sakamoto and his lab members for the time that I spent in the research room. Many thanks also to Prof. Toshio Kasai for allowing me to participate in his research early on in my doctoral studies.

I am also thankful for the financial assistance provided by Japan Student Services Organization (JASSO) and the Matsuda Yosahichi Memorial Foundation for Foreign Students (松田與三七記念留学生奨学基金) during the first half of my study period.

I would like to thank my family, nuclear or otherwise, who continued to support me as best as they can. Additionally, I would also like to thank my friends past and present, who understood my plight and provided many insights. Special thanks are accorded to my friends from my undergraduate days, who continues to believe in me without asking probing questions (in particular taboo questions to doctoral students).

Finally, I have to give my special heartfelt thanks to a special partner, who has suffered untold misery during my study, but always providing support and encouragement, especially during the darkest of times.